Heterogeneous Chemistry of the NO_3 Free Radical and N_2O_5 on Decane Flame Soot at Ambient Temperature: Reaction Products and Kinetics

Federico Karagulian[†] **and Michel J. Rossi***

Laboratoire de Pollution Atmosphérique et Sol (LPAS), Station 6, CH H5, Ecole Polytechnique Fédérale de Lausanne (EPFL), CH-1015 Lausanne, Switzerland

Received: October 29, 2006; In Final Form: January 10, 2007

The interaction of NO_3 free radical and N_2O_5 with laboratory flame soot was investigated in a Knudsen flow reactor at $T = 298$ K equipped with beam-sampling mass spectrometry and in situ REMPI detection of NO_2 and NO. Decane ($C_{10}H_{22}$) has been used as a fuel in a co-flow device for the generation of gray and black soot from a rich and a lean diffusion flame, respectively. The gas-phase reaction products of NO_3 reacting with gray soot were NO, N_2O_5, HONO, and HNO_3 with HONO being absent on black soot. The major loss of NO_3 is adsorption on gray and black soot at yields of 65 and 59%, respectively, and the main gas-phase reaction product is N_2O_5 owing to heterogeneous recombination of NO_3 with NO_2 and NO according to $NO_3 + \{C\} \rightarrow NO +$ products. HONO was quantitatively accounted for by the interaction of NO_2 with gray soot in agreement with previous work. Product N_2O_5 was generated through heterogeneous recombination of NO_3 with excess NO_2, and the small quantity of HNO_3 was explained by heterogeneous hydrolysis of N_2O_5. The reaction products of N_2O_5 on both types of soot were equimolar amounts of NO and NO_2, which suggest the reaction $N_2O_5 + \{C\} \rightarrow N_2O_{3(ads)} +$ products with $N_2O_{3(ads)}$ decomposing into $NO + NO_2$. The initial and steady-state uptake coefficients γ_0 and γ_{ss} of both NO_3 and N_2O_5 based on the geometric surface area continuously increase with decreasing concentration at a concentration threshold for both types of soot. γ_{ss} of NO_3 extrapolated to $[NO_3] \rightarrow 0$ is independent of the type of soot and is 0.33 ± 0.06 whereas γ_{ss} for $[N_2O_5] \rightarrow 0$ is $(2.7 \pm 1.0) \times 10^{-2}$ and $(5.2 \pm 0.2) \times 10^{-2}$ for gray and black soot, respectively. Above the concentration threshold of both NO_3 and N_2O_5, γ_{ss} is independent of concentration with $\gamma_{ss}(NO_3) = 5.0 \times 10^{-2}$ and $\gamma_{ss}(N_2O_5) = 5.0 \times 10^{-3}$. The inverse concentration dependence of γ below the concentration threshold reveals a complex reaction mechanism for both NO_3 and N_2O_5. The atmospheric significance of these results is briefly discussed.

1. Introduction

Atmospheric aerosols are recognized to be important as a global climate factor whose uncertainty has given rise to numerous climate change scenarios for time horizons of 50−100 years.[1] In addition, they may affect the atmospheric composition through their interaction with trace gases in cases where they attain significant surface-to-volume ratios that enable many heterogeneous or multiphase reactions. Soot is a significant component of many atmospheric aerosols[2−4] that plays a unique role for several reasons. Despite the hydrophobic nature of freshly emitted soot, it is thought to cause cloud formation processes by providing cloud condensation (CCN) or ice (IN) nuclei depending on the age, and thus surface composition, of the aerosol particles[5] and is therefore an important factor in global climate change.[6] In addition, it is the only globally occurring aerosol that has strong absorbing properties from the near IR to the UV spectral range and therefore significantly affects the global radiative balance by absorbing both terrestrial (long wave) as well as solar (short wave) components of the actinic spectrum.[7,8] Soot particles have reducing properties and therefore generate interesting reaction products such as HONO not normally resulting from gas-phase processes in the oxidizing atmosphere.[9−12] These reaction products of intermediate oxidation state can then bring about other redox reactions not possible without the occurrence of reducing soot particles. There exist many heterogeneous chemical reactions involving carbonaceous particles of soot substrates of potential relevance to the atmosphere that have been compiled and evaluated in the past.[13] Last, combustion aerosol emitted into the boundary layer has been recently recognized to be a public health issue.[14,15]

Soot is a carbon-containing aerosol resulting from incomplete combustion of hydrocarbon fuel of varying stoichiometry, defined by the λ-ratio of fuel to oxygen. Soot usually implies only the condensed phase and excludes the volatile organic fraction as well as the surrounding gas phase. It is formed through a complex network of chemical processes from small C_2-C_4 hydrocarbon fragment free radicals that results in large stacked molecular condensates that in part contain substituted aromatic structures depending on the combustion conditions.[16−18] Despite long-standing efforts at elucidating the soot formation mechanism, the molecular details have not emerged yet even though useful structural models have been proposed.[18] Soot particles are composed of insoluble amorphous carbon, sometimes called elemental (EC) or black carbon (BC), and a soluble organic fraction (OC) containing up to 50% of the soot particle mass under certain conditions, of partially oxidized hydrocarbons as a bulk phase associated with the EC core or forming an adsorbed layer on the particle surface.[16] This soluble OC fraction

* To whom correspondence should be addressed. E-mail: michel.rossi@epfl.ch or mj.rossi@bluemail.ch.

[†] Present address: Department of Chemistry, UC Irvine, Irvine, CA 92697-2025.

10.1021/jp0670891 CCC: $37.00
Published on Web 02/22/2007

may span the gamut of high molecular weight compounds from complex organic matter such as humic acid-like substances (HULIS) to highly annellated polycyclic aromatic hydrocarbons whose reactivity with trace gases has been the recent focus of research.[19,20] This organic fraction may play a significant role in the reactivity of soot and may take an active part in the formation of reaction products such as HONO resulting from the reduction of NO_2 on soot according to eq 1.

$$NO_2 + \{C-H\}_{red} \rightarrow HONO + \{C\}_{ox} \quad (1)$$

HONO formation is an example of an interesting reaction product that previous studies have identified as a result of a heterogeneous reaction of NO_2 with soot.[16,21,22,31−39] However, it was conjectured that there must be additional sources of HONO in the atmosphere because the quantities of soot necessary to support the observed levels of atmospheric HONO are not sufficient. Three recent examples are the light-supported (actinic) formation of HONO in the presence of humic acids that are ubiquitous in the environment,[40] the generation of HONO from irradiated nitrate-containing ice in a hitherto unknown reaction mechanism,[41] and the interaction of NO_2 with NH_4Cl aerosol.[42] It is very likely that there are several significant additional day and/or nighttime sources of HONO. The present work contributes an additional mechanism of HONO formation in the presence of N_2O_5 and a specific type of soot substrate.

The primary particle size of soot aerosol may range from 10 to 150 nm and a lifetime of several to tens of days before being scavenged in wet deposition processes. During their lifetime as suspended aerosol they are actively partaking in heterogeneous chemical reactions with gaseous pollutants such as HNO_3, NO_2, and O_3[9,21−23] and therefore reduce oxidized species in the atmosphere. These processes are noncatalytic, consume the reactive sites of soot and thus modify its structure through surface oxidation in a typical aging process that generally leads to an increase of soot surface oxygen functionalities.[16,24−29] Until now, no experimental work has been reported on the interaction of NO_3 on soot in contrast to laboratory experiments of N_2O_5 reacting with soot.[11,47]

The present work deals with the interaction of NO_3 and N_2O_5 with soot substrates from a laboratory combustion aerosol simulating an exhaust gas plume of a combustion engine. Active nitrogen or NO_y, which includes NO_x, is connected to the abundance of global ozone because NO_x directly partakes in atmospheric oxidation processes being a catalytic species, whereas NO_y species act as NO_x reservoir. The relative abundance of NO_x and NO_y in the planetary boundary layer can change significantly with altitude even within 10 m, and with it its characteristic influence on tropospheric ozone.[30]

2. Experimental Method

A custom-designed co-flow system has been used to produce flame soot from decane fuel in a reproducible way.[22] It leads to a diffusion flame maintained in a controlled flow of air. To regulate the fuel flow feeding the flame by capillary forces, two types of ceramics of different porosity were used. One type of soot has been generated in a lean flame (low fuel/oxygen ratio) and will be referred to as "black" soot; the second has been generated in a rich (high fuel/oxygen ratio) and will be referred to as "gray" soot. These correspond to two types of soot obtained under two limiting flame conditions for the given combustion device used whose internal surface measured by BET and elemental composition have been given.[22] Table 1 displays the characteristic parameters we have used to produce the two types of flame soot. The samples were collected from the burnt gases at 1 cm above the visible flame on ambient temperature Pyrex glass plates of 19.6 cm^2 surface area. The different soot substrates used in this work are meant to show the change in the chemical and physical properties of fresh soot emitted into the atmosphere by combustion sources when two limiting conditions of combustion, such as rich vs lean, are chosen.

TABLE 1: Characteristic Parameters of Flame Soot Used To Produce Decane Soot

flame type (decane)	air flow [L min^{-1}]	fuel duct (pore Ø) [μm]	soot type	BET surface area [m^2 g^{-1}][22]	diam of soot particle [nm][21]
rich	1.2−1.4	17−40	"gray"	69	40
lean	1.3−1.5	11−16	"black"	218	20

The reactivity of the soot samples toward NO_3 and N_2O_5 was examined in a low-pressure (Knudsen) flow reactor using modulated molecular beam mass spectrometry (MMBMS) for the measurement of the rate of reactant uptake and product release into the gas phase. To unambiguously monitor the concentration of NO and NO_2 in situ, resonance enhanced multiphoton ionization (REMPI) was employed as part of a multi-diagnostic experimental technique in addition to MMBMS. Design and operation of the Knudsen flow reactor have been described in detail in the literature[43] as well as the in situ REMPI detection of NO and NO_2[44] performed using a Nd:YAG-pumped dye laser. The gas-kinetic parameters of the Knudsen flow reactor as well as details pertaining to in situ REMPI detection of NO and NO_2 may be found in refs 43 and 44. The measurement of molecular flux and concentration was performed using MS and REMPI detection, as reported in previous work.[44]

The mass of soot was varied between 1.5 and 20 mg spread out over 19.6 cm^2. Each sample was pumped for 10 min before performing an uptake experiment. The gas under study, NO_3, was generated by thermal decomposition of N_2O_5 at 530 K in a 6 mm diameter glass tube that directly extends into the reactor. Due to the low residence time and pressure in the reactor, there is no recombination of NO_3 with NO_2 to form N_2O_5. Production of NO_3 and characterization of the NO_3 source have been reported in detail in a recent study.[44] Hydrolysis of N_2O_5 may occur on internal surfaces of the inlet line before flowing across the hot glass tube thus generating HNO_3 as an impurity on the order of a few to 15%. However, HNO_3 does not thermally decompose inside the hot glass tube of the NO_3 source because we did not observe any change in the MS signal amplitude at m/e 63 (HNO_3^+) when increasing the source temperature from ambient to 530 K. Both NO_3 and N_2O_5 were introduced into the reactor as a continuous flow from the NO_3 source which was heated for NO_3 and was run at ambient temperature for N_2O_5. The used free radical NO_3 source consistently generated a 3-fold excess of NO_2 owing to heterogeneous secondary processes of NO_3 to NO_2 within the source, as reported before.[44] This associated and unfortunately unavoidable NO_2 flow is in part responsible for the obtained reaction products (see below).

2.1. NO_3. The relative concentration of NO_3 decreases with decreasing escape orifice diameter because it undergoes increasing wall loss with increasing residence time in the Knudsen reactor. The measured first-order loss of NO_3 given by k' at a given escape orifice size of the reactor may be expressed as the sum of two components, namely, k_{esc} and k_{dec}, representing escape, that is, physical, and chemical loss, respectively: $k' = k_{esc} + k_{dec}$. As reported in recent work,[44] the measurement of k' at three different aperture sizes enabled the determination of $k_{dec} = 0.6 \pm 0.27$ s^{-1} at 300 K. NO_3 has a measurable parent

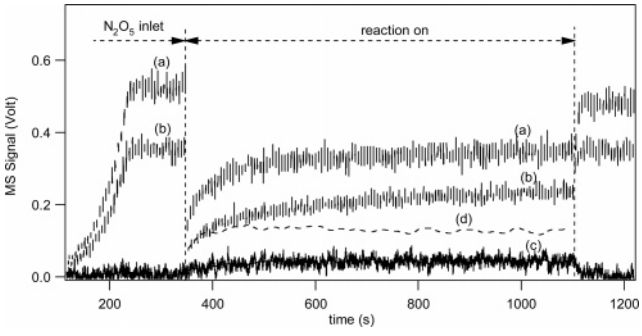

Figure 1. N_2O_5 uptake on a sample of 10 mg of gray soot at $[N_2O_5] = (8.0 \pm 1.3) \times 10^{12}$ cm^{-3} and at an orifice diameter of 4 mm. Curves a and b correspond to the raw MS signals monitored at *m*/*e* 46 and 30, respectively. Curve c corresponds to the raw REMPI signal for NO_2 at $\lambda_{NO_2} = 511$ nm (Coumarin 307, Radiant Dyes) scaled to a MS signal at *m*/*e* 46. Curve d corresponds to the excess MS signal at *m*/*e* 30 related to the production of NO.

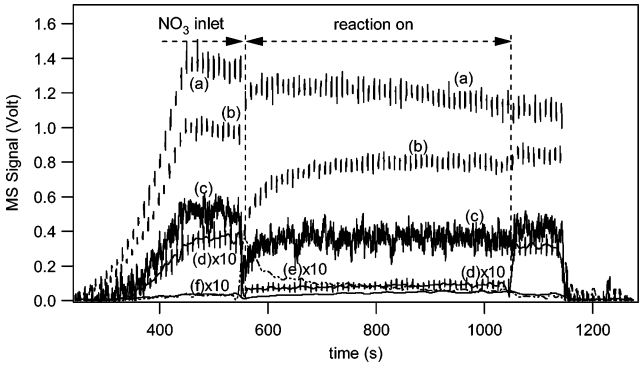

Figure 2. NO_3 uptake on a sample of 10 mg of gray soot at $[NO_3] = (7.0 \pm 1.0) \times 10^{11}$ cm^{-3} in the 8 mm aperture reactor. Curves a, b, and d−f correspond to the raw MS signals monitored at *m*/*e* 30, 46, 62, 47, and 63, respectively. Curve c corresponds to the raw REMPI signal for NO_2 at $\lambda_{NO_2} = 511$ nm scaled to a MS signal at *m*/*e* 46.

peak at *m*/*e* 62 (NO_3^+) denoted as $I_0^{62(NO_3)}$ and $I_r^{62(NO_3)}$ corresponding to the MS signal before and during reaction, respectively. The measured rate constant k_{obs} for NO_3 disappearance from the gas phase is given by eq 2.

$$k_{obs} = \left(\frac{I_0^{62(NO_3)}}{I_r^{62(NO_3)}} - 1\right)(k_{esc} + k_{dec}) \qquad (2)$$

In the following, the subscripts 0 and *r* will refer to continuous gas uptake experiments in the absence and presence, respectively, of the sample. N_2O_5 does not have a measurable parent and fragment peak at *m*/*e* 108 ($N_2O_5^+$) and 62 (NO_3^+), respectively, under the present experimental conditions; the most intense peaks are its fragment NO_2^+ at *m*/*e* 46 followed by the less intense fragment NO^+ at *m*/*e* 30. The details regarding the contribution of the HNO_3 impurity to the MS amplitude at *m*/*e* 46 and 30 may be found in Appendix A1. In the NO_3 uptake experiments only $[NO_2]$ was detected by REMPI whereas [NO] was evaluated at *m*/*e* 30 after successive subtraction of the detected reaction products contributing at *m*/*e* 30 (see eq A2 in Appendix A1).

2.2. N_2O_5. When N_2O_5 is exposed to soot, it is taken up and undergoes a heterogeneous reaction which results in a decrease of the MS signal from $I_0^{46(N_2O_5)}$ to $I_r^{46(N_2O_5)}$. Upon N_2O_5 uptake on both gray and black soot, we observe the formation of both NO and NO_2 in the gas phase as detected by in situ REMPI at $\lambda = 452.5$ and 511 nm, respectively. For NO_2 REMPI detection a Coumarin 307 (Radiant Dyes) methanol solution was used whereas NO was multiphoton ionized using a methanol solution of Coumarin 47 (Radiant Dyes). We have determined the rate constant k_{obs} for the disappearance of N_2O_5 following eq 3, assuming that the rate law is first order in N_2O_5,

$$k_{obs} = \left(\frac{I_0^{46(N_2O_5)}}{I_r^{46(N_2O_5)}} - 1\right)k_{esc} \qquad (3)$$

where $I_0^{46(N_2O_5)}$ and $I_r^{46(N_2O_5)}$ are the intensities of the NO_2^+ fragment of N_2O_5 before and during heterogeneous reaction, respectively, and k_{esc} is the measured rate constant of effusion for N_2O_5 out of the flow reactor. To determine $I_r^{46(N_2O_5)}$, the raw MS signal at *m*/*e* 46 was corrected for the product NO_2 generated during uptake of N_2O_5 on soot because NO_2 contributes to the total MS signal I_r^{46} at *m*/*e* 46, its parent peak.[45] Figure 1 shows the raw REMPI signal at $\lambda = 511$ nm corresponding to NO_2 production for a typical uptake experiment of N_2O_5 on soot scaled to a MS signal amplitude and thus to a flow rate. For both uptake experiments performed with NO_3 and N_2O_5 the absolute NO_2 concentration, $[NO_2]_{0,r}$, in the absence and presence of the soot sample, respectively, has been determined by means of in situ REMPI detection of NO_2[44]. The procedure used to calculate its MS signal contribution $I_{0,r(REMPI)}^{46(NO_2)}$ at *m*/*e* 46 in the absence (subscript "0") and presence (subscript "r") of the soot sample has been reported in Appendix A2.

If one assumes that the rate law for uptake is first order, the uptake coefficient γ_{obs} for NO_3 and N_2O_5 is given by $\gamma_{obs} = k_{obs}/\omega$, where ω is the collision frequency of N_2O_5 or NO_3 with the soot sample. In the present data analysis γ_{obs} was calculated using the geometric surface area A_s of the sample holder which will be justified below; γ_{obs} became γ_{ss}, the steady-state uptake coefficient, once steady-state conditions were achieved after an exposure time of 500 s or so; γ_{obs} is γ_0 at $t = 0$ s, that is, immediately after lifting the plunger and thus exposing the soot sample to N_2O_5. The details of the product analysis arising from the heterogeneous reaction of N_2O_5 on soot may be found in Appendix A2.

Continuous flow uptake experiments were carried out at ambient temperature (298 ± 2 K) under molecular flow conditions. The concentration of NO_3 inside the Knudsen reactor ranged between $(2.7 \pm 0.5) \times 10^{11}$ cm^{-3} and $(2.4 \pm 0.5) \times 10^{12}$ cm^{-3}. The associated $[NO_2]$ without reaction on soot determined by REMPI was $(8.0 \pm 1.0) \times 10^{11}$ cm^{-3} for the lower limit of $[NO_3] = (2.7 \pm 0.5) \times 10^{11}$ cm^{-3} and $(6.2 \pm 1.5) \times 10^{12}$ cm^{-3} for the upper limit of $[NO_3] = (2.4 \pm 0.5) \times 10^{12}$ cm^{-3}.

3. Results and Discussion

3.1. NO_3 Reaction with Gray Decane Soot: Reaction Products. The interaction of NO_3 with gray decane soot was investigated in a series of uptake experiments performed at different masses of soot and at different $[NO_3]$. Figure 2 shows a typical uptake experiment of NO_3 on 10 mg of gray soot at $[NO_3] = (7.0 \pm 1.0) \times 10^{11}$ cm^{-3}. Once a steady flow of NO_3 was established, the isolation plunger was lifted at $t = 550$ s and the substrate exposed to the NO_3 flow. Because of the uptake of NO_3 on soot, the number of molecules effusing through the escape orifice and thus the MS signal at *m*/*e* 62 immediately decreases (curve d). At $t = 1050$ s the sample compartment is sealed by lowering the plunger and the MS signal at *m*/*e* 62 returns to its initial value. The slight decrease

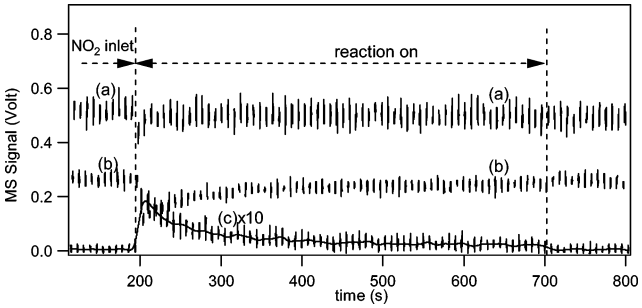

Figure 3. NO_2 uptake on a sample of 10 mg of gray soot at $[NO_2] = (2.3 \pm 0.5) \times 10^{12}$ cm^{-3} (orifice diameter = 8 mm). Curves a−c correspond to the raw MS signals monitored at *m*/*e* 30, 46, and 47, respectively. Curve c describes HONO production.

of $I_0^{62(NO_3)}$ over extended periods of time such as displayed in Figure 2 may be explained by a slight decrease of the corresponding flow rate into the reactor. In all experiments we observed uptake of NO_2 that only occurred in the presence of NO_3, which led to a net decrease of the REMPI signal for NO_2 at $\lambda_{NO_2} = 511$ nm (Figure 2, curve c). The major loss of NO_3 is simple adsorption on gray and black soot. We did not perform experiments at higher temperatures to measure the reversibility of the reaction of NO_3 with soot.

NO_2 in the absence of soot arises from the thermal decomposition of N_2O_5 and NO_3 in the NO_3 source or in the flow reactor. Reference uptake experiments with pure NO_2 in the presence of gray soot were performed at $[NO_2] = (2.3 \pm 0.5) \times 10^{12}$ cm^{-3} (Figure 3). A large and instantaneous rate of uptake was observed and attained steady-state conditions after 3 min of interaction. The initial and steady-state uptake coefficients were $\gamma_0 = (3.0 \pm 0.6) \times 10^{-2}$ and $\gamma_{ss} = (1.3 \pm 0.2) \times 10^{-3}$, respectively, and were similar to previous results.[32,34] Simultaneously to the uptake of NO_2 a large product peak of HONO appears, which shows that the conversion of NO_2 into HONO is a fast process (Figure 3, curve c). The observed HONO yields defined as the ratio of the integral of HONO released to the amount of NO_2 taken up during the reaction time tended toward 100 ± 10% and were independent of integration time (Figure 3). No significant formation of NO was observed.

Identical behavior has been observed at low $[NO_2]$ in recent work on the reactivity of NO_2 on decane flame soot[22] and confirms that NO_2 strongly interacts with flame soot. This is in contrast to uptake experiments of NO_2 on mineral dust, which showed that NO_2 does not significantly adsorb on dust except on Saharan dust.[44] In that case NO_2 reacted only on NO_3 that was previously adsorbed on the substrate which has also been observed on the present soot substrate (see below).

During the uptake of NO_3 on gray soot the MS signal at *m*/*e* 62 (Figure 4a, curve a) partially recovered as the exposure time increases, indicating a decrease in the rate of uptake of NO_3, presumably owing to a decrease of the net number of available surface sites for reaction. As a consequence, we observe an apparent reduction of the uptake coefficient γ_{ss}. As displayed in Figure 4a, a large burst of HONO at *m*/*e* 47 co-incident with the uptake of NO_3 has been observed immediately after the exposure of the sample which reaches steady state after 500 s (Figure 4a, curve b). NO has been observed at the beginning of the reaction and tended to small values at steady-state conditions (Figure 4a, curve c). A fast initial rate of formation of HONO and NO is observed immediately after exposure of soot to NO_3 as displayed in Figure 4a, curves b and c. Following results with pure NO_2 interacting with the same type of soot as displayed in Figure 3 the observed HONO formation is attributed

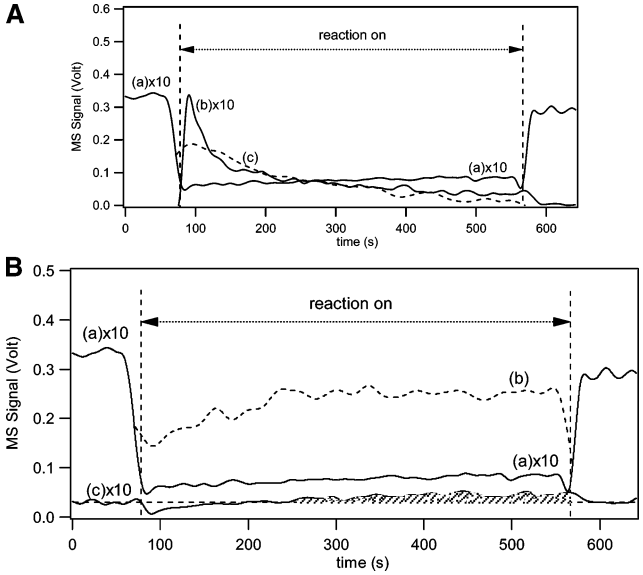

Figure 4. (a) Uptake of NO_3 on 10 mg of gray decane soot and resulting reaction products at $[NO_3] = (7.0 \pm 1.0) \times 10^{11}$ molecule cm^{-3} from data displayed in Figure 2 that are electronically smoothed and interpolated (orifice diameter = 8 mm). Curve a represents the raw MS signal at *m*/*e* 62 for the NO_3 uptake on the soot sample. Curve b represents the raw MS signal at *m*/*e* 47 related to the production of gas-phase HONO. Curve c represents the corrected MS signal at *m*/*e* 30 corresponding to the production of gas-phase NO. (b) Uptake of NO_3 on 10 mg of gray soot and resulting reaction products at $[NO_3] = (7.0 \pm 1.0) \times 10^{11}$ molecule cm^{-3} (from experiment displayed in Figure 2 but electronically smoothed and interpolated, orifice diameter = 8 mm). Curve a represents the raw MS signal at *m*/*e* 62 for the NO_3 uptake on the soot sample. Curve b is the calculated MS signal at *m*/*e* 46, I_{exc}^{46}, corresponding to N_2O_5 formation. Curve c represents the raw MS signal at *m*/*e* 63 for the impurity HNO_3 uptake on soot. Positive flow MS signal at *m*/*e* 63 indicated by the hatched area under curve c represents the net amount of generated HNO_3.

to the reduction of NO_2 by reducing sites on gray soot according to reactions 4a and 4b.[34,46]

$$NO_2 \rightarrow NO_{2(ads)} \quad (4a)$$

$$NO_{2(ads)} \text{ or } NO_2 + \{C-H\}_{red} \rightarrow HONO + \{C\}_{ox} \quad (4b)$$

The species listed in curved brackets refer to surface adsorbates. $\{C-H\}_{red}$ represents a surface site on gray soot that reduces NO_2 to HONO and $\{C\}_{ox}$ is the reaction product after surface oxidation by NO_2 on soot. The interaction of NO_2 with an adsorption site in reaction 4a must be weak to be sufficiently mobile to subsequently interact with other surface sites for reaction 4b in a Langmuir−Hinshelwood mechanism.

For all gray and black soot samples we have observed the formation of small amounts of gas-phase N_2O_5. We have calculated the yield of N_2O_5 from the increase of the corrected MS signal at *m*/*e* 46, I_{exc}^{46}, discussed in Appendix A2 and displayed in Figure 4b (curve b). The yield of N_2O_5 following the uptake of NO_3 continuously increases and reaches steady state after 500 s.

Under our experimental conditions the formation of N_2O_5 may be explained by NO_2 reacting with adsorbed NO_3 on the soot substrate. It is important to note that NO_2 itself reacts both on gray and on black decane soot.[22,32] The observed simultaneous uptake for both NO_3 and NO_2 suggests the formation of $N_2O_{5(ads)}$ through the heterogeneous recombination reaction 5a.

$$NO_{3(ads)} + NO_{2(ads)} \rightarrow N_2O_{5(ads)} \quad (5a)$$

TABLE 2: Summary Yields of Reaction Products during the Heterogeneous Reaction of NO_3 on Decane Soot Samples of 19.6 cm^2 Geometric Surface Area at $[NO_3]_0 = (2.3 \pm 0.5) \times 10^{12}$ cm^{-3} and $[NO_2]_0 = (6.0 \pm 1.0) \times 10^{12}$ cm^{-3} (Orifice Diameter = 8 mm)[e,f]

gray soot (decane)	5 mg	% yield	10 mg	% yield	20 mg	% yield	average yield[d]	% yield[g]
$NO_{3(lost)}$	$(3.2 \pm 0.7) \times 10^{18}$		$(3.3 \pm 0.7) \times 10^{18}$		$(3.3 \pm 0.7) \times 10^{18}$		$(3.3 \pm 0.7) \times 10^{18}$	
$N_2O_{5(g)}$	$(7.0 \pm 1.7) \times 10^{17}$ [a]	22	$(8.5 \pm 1.4) \times 10^{17}$ [a]	25	$(8.4 \pm 1.2) \times 10^{17}$ [a]	22	$(8.5 \pm 1.4) \times 10^{17}$ [a]	23 ± 7
$NO_{2(lost)}$	$(2.4 \pm 0.6) \times 10^{18}$		$(2.5 \pm 0.5) \times 10^{18}$		$(3.7 \pm 0.7) \times 10^{18}$		$(3.1 \pm 0.6) \times 10^{18}$	
$NO_{(g)}$	$(3.2 \pm 0.5) \times 10^{17}$ [a]	10	$(3.3 \pm 0.7) \times 10^{17}$ [a]	10	$(4.6 \pm 1.0) \times 10^{17}$ [a]	13	$(4.0 \pm 0.9) \times 10^{17}$ [a]	11 ± 5
$HNO_{3(g)}$	$(4.8 \pm 0.5) \times 10^{16}$ [a]	1.5	$(5.0 \pm 0.3) \times 10^{16}$ [a]	1.5	$(6.6 \pm 0.6) \times 10^{16}$ [a]	2	$(5.8 \pm 1.0) \times 10^{16}$ [a]	1.8 ± 0.5
$HONO_{(g)}$	$(1.6 \pm 0.2) \times 10^{18}$ [b]	94	$(1.6 \pm 0.5) \times 10^{18}$ [b]	98	$(2.5 \pm 0.8) \times 10^{18}$ [b]	87	$(2.0 \pm 0.7) \times 10^{18}$ [b]	96 ± 8
black soot (decane)	5 mg	% yield	10 mg	% yield	20 mg	% yield	average yield[d]	% yield[g]
$NO_{3(lost)}$	$(3.2 \pm 0.5) \times 10^{18}$		$(3.4 \pm 0.8) \times 10^{18}$		$(3.5 \pm 0.5) \times 10^{18}$		$(3.5 \pm 0.5) \times 10^{18}$	
$N_2O_{5(g)}$	$(1.0 \pm 0.6) \times 10^{18}$ [a]	31	$(7.2 \pm 1.2) \times 10^{17}$ [a]	20	$(7.0 \pm 1.0) \times 10^{17}$ [a]	20	$(7.0 \pm 1.0) \times 10^{17}$ [a]	24 ± 7
$NO_{2(lost)}$	$(2.8 \pm 0.4) \times 10^{18}$		$(3.0 \pm 0.6) \times 10^{18}$		$(3.0 \pm 0.8) \times 10^{18}$		$(3.0 \pm 0.6) \times 10^{18}$	
$NO_{(g)}$	$(4.5 \pm 0.7) \times 10^{17}$ [a]	14	$(5.1 \pm 0.4) \times 10^{17}$ [a]	15	$(6.3 \pm 0.5) \times 10^{17}$ [a]	18	$(5.7 \pm 0.5) \times 10^{17}$ [a]	16 ± 6
$HNO_{3(g)}$	$(4.8 \pm 0.5) \times 10^{16}$ [a]	1.5	$(6.8 \pm 0.7) \times 10^{16}$ [a]	2	$(5.2 \pm 0.5) \times 10^{16}$ [a]	1.5	$(6.0 \pm 0.7) \times 10^{16}$ [a]	1.6 ± 0.4
$HONO_{(g)}$	−[c]		−		−		−	

[a] Yield of NO_y given as percentage with respect to the total number of molecules of NO_3 taken up on soot during a reaction time of 500 s. [b] Yield of HONO given as a percentage with respect to the total number of molecules of $NO_{2(lost)} - N_2O_{5(g)}$ taken up during a reaction time of 500 s.[c] Dash (−) indicates that no reaction product has been observed. [d] The average yield is calculated on the basis of the results obtained for 10 and 20 mg of soot corresponding to a coherent soot layer. [e] The average uncertainty of the yields is ±20%. [f] Uncertainty includes systematic error. [g] Includes a potential systematic uncertainty for N_2O_5 and NO owing to successive subtraction (see eqs A1 and A2).

The conversion of NO_3 to N_2O_5 occurs via a Langmuir−Hinshelwood mechanism where NO_3 and NO_2 first adsorb onto the soot surface and subsequently react forming N_2O_5 which in part desorbs from the surface.

Once N_2O_5 has been formed in the adsorbed state, a fraction may desorb into the gas phase, and another may subsequently react, as will be discussed below in section 3.3.

$$N_2O_{5(ads)} \rightarrow N_2O_{5(g)} \qquad (5b)$$

HNO_3, present as an impurity, reacts on the soot substrate as well. This reaction has been studied in recent laboratory work using the same experimental apparatus.[23] As displayed in Figure 4b, a significant initial uptake of HNO_3 was observed at *m*/*e* 63 (curve c). After a reaction time of 170 s, an excess in the MS signal at *m*/*e* 63 corresponding to formation rather than loss of HNO_3 is observed, as indicated by the hatched area in Figure 4b, curve c. The increasing rate of formation of HNO_3 in the presence of soot coincides with the trend of N_2O_5 formation displayed in Figure 4b, curve b and shows that part of $N_2O_{5(ads)}$ formed in reaction 5a undergoes hydrolysis on the surface of soot. HNO_3 is then released back into the gas phase after heterogeneous hydrolysis, reaction 6.

$$N_2O_{5(ads)} + H_2O_{(ads)} \rightarrow 2HNO_{3(g)} \qquad (6)$$

The yield of HNO_3 observed in uptake experiments performed at $[NO_3] = (2.5 \pm 0.5) \times 10^{12}$ cm^{-3} on different amounts of gray and black soot is only 1.5−2% of the total number of NO_3 molecules taken up (see Table 2).

An increase of gas-phase HNO_3 formation in the presence of soot aerosol has been observed in recent experimental work at very low humidities in which NO_2, HNO_3, and NO_3/N_2O_5 reacted on soot particles in a large aerosol chamber.[11] In the same study the reaction probability for reaction 6 was assumed to be time independent and resulted in $\gamma = (4.0 \pm 2.0) \times 10^{-5}$. Apparently there exists sufficient adsorbed water even at low relative humidity to enable reaction 6 such that H_2O is not the limiting reagent.

In Table 2 we report the product yields for the NO_3 reaction on three different masses of gray soot at $[NO_3] = (2.5 \pm 0.5) \times 10^{12}$ and an excess of NO_2 of $(6.0 \pm 1.0) \times 10^{12}$ cm^{-3}. We point out that the experimental uncertainties for N_2O_5 and NO reported in the last column of Table 2 also include potential systematic errors owing to the evaluation of the product yields by successive subtraction (see eqs A1 and A2). The mass balance reveals that 16−30% of NO_2 taken up on gray soot has been converted into gas-phase N_2O_5 according to reactions 5a and 5b under the assumption of excess adsorbed NO_3 that is converted only in moderate yields to gas-phase NO (see below). The remaining 70−84% of reacted NO_2 equals the yield of HONO produced due to reaction 4b according to the NO_2 mass balance, namely $N(N_2O_5) + N(HONO) = N(NO_2)$, where N is the number of molecules taken up after a given reaction time. The essentially 100% yield of HONO resulting from pure NO_2/gray soot experiments, in agreement with previous results,[22] leads to the amount of generated N_2O_5 calculated from the amount of NO_2 taken up minus the yield of N_2O_5. We may conclude that NO_3 reacting on gray soot does not generate HONO because the amount of HONO may be entirely accounted for by the loss of NO_2. Therefore, the slow production of NO must be attributed to the reaction of NO_3 with gray soot. Previous work has shown that HONO is the only gas-phase product from the reaction of pure NO_2 with gray soot[22,34] in contrast to NO formation resulting from the NO_2 reaction on amorphous carbon[32] or black soot (see below). Therefore, we attribute the slow formation of NO exclusively to the heterogeneous reaction of NO_3 on gray soot according to reaction 7 knowing that NO_2 does not lead to NO on gray soot.

$$NO_3 + \text{soot} \rightarrow NO + \text{products} \qquad (7)$$

The amount of NO released into the gas phase has been calculated from the excess MS signal at *m*/*e* 30, I_{exc}^{30} according to eq A2. The yield of NO did not show a significant variation with $[NO_3]$ and the amount of soot. Table 2 displays the fact that NO corresponds to nearly 6−16% of NO_3 taken up on the substrate. In addition, NO is nonreactive toward fresh unexposed soot samples,[22,32] a result obtained in ancillary experiments for the present soot samples.

To explain the temporal trend of the observed product yields on gray soot displayed in Figure 4, we need to analyze the time dependence of reactants and products at the beginning (between

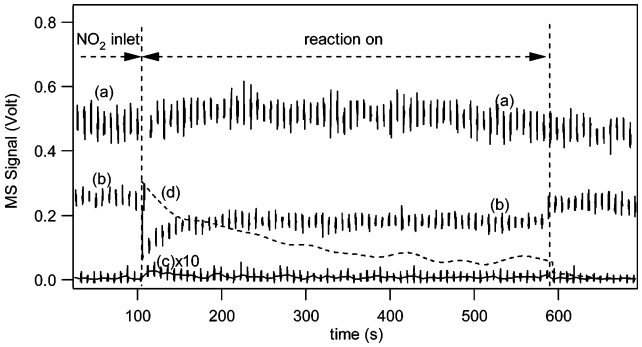

Figure 5. NO_2 uptake on a sample of 10 mg of black soot at $[NO_2] = (2.3 \pm 0.5) \times 10^{12}$ cm^{-3} (orifice diameter = 8 mm). Curves a−c correspond to the raw MS signals monitored at *m*/*e* 30, 46 and 47, respectively. Curve d (broken line) reports the NO formation.

t = 62 and 210 s) and at t > 210 s of the uptake process, respectively. At first the fast disappearance of gas-phase NO_2 leads to fast HONO production (curve b in Figure 4a, reaction 4b). Concurrently, the fast uptake of NO_3 leads to rapid decomposition on the substrate resulting in a significant rate of formation of NO (curve c in Figure 4a, reaction 7). Therefore, owing to competitive reactions 4b and 7, only a fraction of $NO_{3(ads)}$ reacts with NO_2 and recombines to N_2O_5 according to reaction 5a whereas all of the NO_2 reacts either to HONO or to N_2O_5. At t > 210 s the number of adsorbed NO_3 molecules increases, thereby leading to partial saturation of the NO_3 uptake and thus inhibiting the turnover of available surface sites where NO_3 decomposition can take place. Therefore, reactions 5a and 5b become predominant with respect to reactions 4b and 7 at later reaction times. On the other hand, HONO production is ongoing in the steady state by continuous NO_2 reaction on gray soot, in contrast to NO production according to reaction 7.

We therefore conclude that according to Table 2 approximately 35 ± 10% of NO_3, which reacted on gray soot has been converted to N_2O_5 and NO. The remaining amount of NO_3, that is, 65 ± 10%, is irreversibly taken up on the substrate. However, no saturation of the uptake of NO_3 has been observed under the current experimental conditions despite the vanishing NO production at late reaction times, as displayed in Figure 4a.

3.2. NO_3 Reaction with Black Decane Soot. The reaction of NO_3 on black soot was examined in the same manner as gray soot discussed above. A fast initial uptake coefficient γ_0 was observed for all experiments performed within $[NO_3]$, which ranged between $(2.7 \pm 0.5) \times 10^{11}$ and $(2.3 \pm 0.5) \times 10^{12}$ cm^{-3}, as reported in Table 2.

Ancillary uptake experiments with pure NO_2 in the presence of black soot were performed at $[NO_2] = (2.3 \pm 0.5) \times 10^{12}$ cm^{-3}. As observed in the companion experiment with gray soot, the observed uptake of NO_2 attained steady-state conditions after 3 min of interaction. The initial and steady-state uptake coefficient was $\gamma_0 = (1.5 \pm 1.0) \times 10^{-2}$ and $\gamma_{ss} = (2.7 \pm 0.6) \times 10^{-3}$, respectively, similar to previous results.[22,32] Simultaneous to the uptake of NO_2 a significant quantity of product NO appears. The amount of product NO has been calculated from the excess MS signal at *m*/*e* 30, I^{30}_{exc}, according to eq A2. This signal has been converted to a flow rate using a calibration factor for pure NO and subsequently integrated over the reaction time. The observed NO yields defined as the ratio of the amount of NO released to the amount of NO_2 taken up during the reaction time tended toward 40% in contrast to the vanishing yield of HONO (Figure 5). Similar behavior at low $[NO_2]$ was

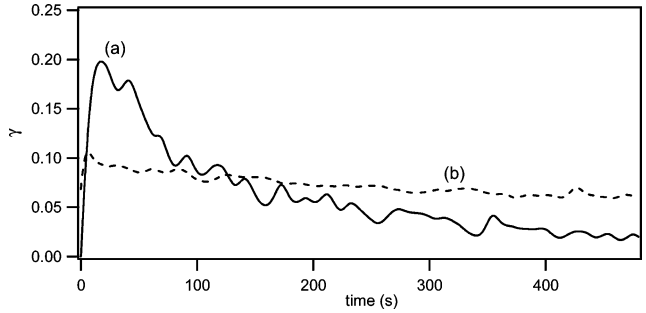

Figure 6. Uptake coefficient γ vs time for NO_3 on 10 mg of black (a) and gray (b) soot. $[NO_3] = (7.0 \pm 1.0) \times 10^{11}$ cm^{-3} (orifice diameter = 8 mm).

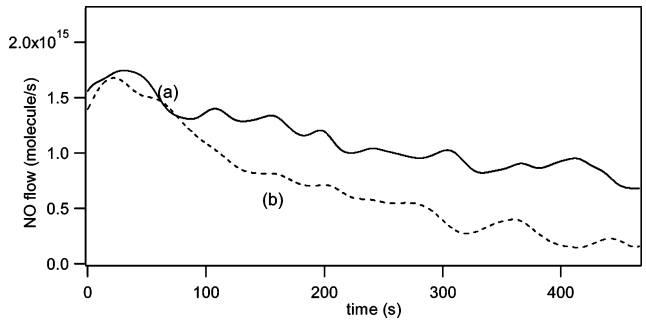

Figure 7. NO rate of formation vs time for NO_3 on 10 mg of (a) black and (b) gray soot. $[NO_3] = (7.0 \pm 1.0) \times 10^{11}$ cm^{-3} (orifice diameter = 8 mm).

observed in recent work on the reactivity of NO_2 on black decane flame soot.[22]

Figure 6 shows the temporal variation of γ for NO_3 on a 10 mg sample of black and gray soot at $[NO_3] = (7.0 \pm 1.0) \times 10^{11}$ cm^{-3} in the presence of NO_2. The value of γ_0 for black soot is twice that observed for gray soot, as will be discussed below. At steady-state conditions the situation is reversed, where γ_{ss} for black soot is smaller by a factor of 2 with respect to γ_{ss} for gray soot. However, the number of NO_3 molecules taken up on both substrates during the exposure time of 500 s is approximately the same. As already observed for gray soot, simultaneous uptake of both NO_3 and NO_2 on black soot leads to the formation of small amounts of gas-phase N_2O_5 according to reactions 5a and 5b.

Figure 7 displays the NO product flow generated during uptake of NO_3 on 10 mg of black and gray decane soot at the same experimental conditions. NO_2 effusing from the hot NO_3 source reacts with black soot to produce mainly NO, as observed in the interaction of NO_2 with amorphous carbon[32] or black decane soot.[22] NO_2 presumably interacts with black soot, resulting in the formation of HONO akin to the reaction on gray soot, which to a large extent decomposes into NO according to the following reaction mechanism proposed by Stadler and Rossi:[22]

$$NO_2 + \{C - H\}_{red} \rightarrow HONO_{(ads)} + \{C\}_{ox} \qquad (4b)$$

$$2HONO_{(ads)} \rightarrow NO + NO_{2(ads)} + (H_2O)_{ads} \qquad (8)$$

The difference in the NO yields between black and gray decane flame soot following reaction with NO_3, curves a and b in Figure 7 is related to the NO formation from HONO decomposition, reactions 4b and 8. NO from HONO decomposition, reaction 8, may therefore occur in addition to the NO formation from heterogeneous decomposition of NO_3 on black soot according to reaction 7 in contrast to gray soot where

TABLE 3: Summary of NO Yield Resulting from the Uptake of NO_3 on 10 mg of Gray and Black Soot at Different $[NO_3]$ (Orifice Diameter = 8 mm)

$[NO_3]_0$, cm^{-3}	NO (gray soot)[a]	% yield	NO (black soot)[a]	% yield
$(2.7 \pm 0.5) \times 10^{11}$	$(1.6 \pm 0.4) \times 10^{17}$	13	$(2.0 \pm 0.5) \times 10^{17}$	20
$(3.8 \pm 1.8) \times 10^{11}$	$(2.0 \pm 0.6) \times 10^{17}$	11	$(2.6 \pm 0.7) \times 10^{17}$	19
$(7.0 \pm 1.0) \times 10^{11}$	$(2.6 \pm 0.5) \times 10^{17}$	9	$(4.3 \pm 0.4) \times 10^{17}$	16
$(1.5 \pm 0.5) \times 10^{12}$	$(3.0 \pm 0.7) \times 10^{17}$	8	$(5.8 \pm 0.8) \times 10^{17}$	14
$(2.3 \pm 0.5) \times 10^{12}$	$(3.3 \pm 0.4) \times 10^{17}$	10	$(5.1 \pm 0.7) \times 10^{17}$	15

[a] Yield of NO given as a percentage with respect to the total number of molecules of NO_3 taken up during the reaction time of 500 s.

HONO is kinetically stable and where NO exclusively stems from reaction 7. Therefore, contributions of NO formation from HONO and NO_3 decomposition cannot be experimentally separated for black in contrast to gray decane soot. Table 4 reveals a NO yield higher by approximately 50% for black compared to gray decane soot that is consistent with the HONO decomposition leading to additional NO in the case of black decane soot.

In recent work performed by Stadler,[22] black decane soot was exposed to a flow of pure HONO to decide whether or not HONO produced on black soot may irreversibly adsorb on the surface or decompose to NO. In that work fast uptake of HONO and production of NO was observed according to reaction 8. The total NO product yield at limiting high concentration was 50% with respect to HONO taken up, whereas for $[HONO] = (3.7 \pm 0.4) \times 10^{11}$ cm^{-3} the total product yield consisted of 40% NO and 10% NO_2. The open balance of nitrogen was attributed to a reservoir of HONO or its reaction product adsorbed on the soot substrate. The NO rate of formation resulting from NO_3 decomposition on gray soot tends to zero under steady-state conditions, as shown in Figure 7, whereas the rate of NO formation on black soot is sustained owing to continuous HONO decomposition following reaction 8. Table 2 reveals that the sum of the yields of NO and N_2O_5 directly attributable to the reaction of NO_3 on black soot amounts to 40 $\pm$ 10% based on NO_3 taken up, a value that is quite comparable to that on gray soot when the contribution of HNO_3 is ignored (1.8% yield). The remainder of adsorbed NO_3, namely 60 $\pm$ 10% must stay adsorbed on the black soot substrate.

Table 3 reports the NO yield resulting from the uptake of NO_3 on 10 mg of gray and black decane soot at $[NO_3]$ between $(2.7 \pm 0.5) \times 10^{11}$ and $(2.3 \pm 0.5) \times 10^{12}$ cm^{-3}. The yield of NO for black soot over an integration period of 500 s was 5−8% larger than for gray soot. There is no significant dependence of the NO yields on $[NO_3]$. The NO yield expressed as a percentage with respect to the total number of molecules of NO_3 taken up during the same reaction time resulted in a value of 10.2 $\pm$ 1.9% for gray and 16.8 $\pm$ 2.6% for black soot when averaged over uptake experiments at different values of $[NO_3]$. We attribute the larger value of the NO yield found for black compared to gray soot to HONO decomposition on black soot. The small difference in the NO yields reported in Table 3 suggests that most of the putative HONO remains adsorbed on black soot rather than decompose to form NO. In agreement with this conclusion, the HONO rate of formation is negligible for the interaction of NO_2 with black soot, as displayed in Figure 5, curve c.

3.3. N_2O_5 Reaction with Decane Soot: Reaction Products. As far as the experimental arrangement is concerned, the only difference between the NO_3 and N_2O_5 uptake experiments was that the source temperature was raised to 530 K for NO_3 whereas it was kept at ambient temperature for N_2O_5. Figures 1 and 8 display typical uptake experiments of N_2O_5 on gray and black soot, respectively. Both NO and NO_2 were detected as the only reaction products resulting from the interaction of N_2O_5 with soot. Figure 1 shows that the NO_2 concentration measured using REMPI detection is zero within experimental uncertainty before exposure of N_2O_5 to soot at $t = 350$ s, which is proof for the absence of NO_2 in the N_2O_5 flow emanating from the source. The same is true for the NO displayed in Figure 8 where REMPI detection of NO was employed. Owing to the dye change for the REMPI detection of NO and NO_2, simultaneous REMPI detection of both reaction products was not possible such that separate uptake experiments using identical $[NO_3]$ had to be undertaken, one set for NO and another for NO_2 detection. However, analysis of the MS signal amplitudes at *m*/*e* 30 and 46 after correction for the contribution of N_2O_5 and NO_2 detected by REMPI following the procedure outlined in Appendix A2 based on I_{exc}^{30}, revealed the presence of NO as a reaction product (see eq A6). Conversely, the MS signal amplitudes at *m*/*e* 30 and 46 revealed the presence of NO_2 as a reaction product once the contribution of N_2O_5 and NO whose absolute concentration was measured using REMPI were accounted for (see eq A5). Qualitatively one observes an increase of both NO and NO_2 during the first 100 s or so after exposing the soot to the N_2O_5 flow that is roughly co-incident with the establishment of steady-state conditions of the MS signal at *m*/*e* 46. This indicates that a certain amount of N_2O_5 must first be adsorbed onto soot before the rate of product desorption becomes significant. We also note that unlike the situation for NO_3 the differences between gray and black soot are minimal.

Table 4 displays the quantitative aspects in terms of the yields of NO and NO_2 using REMPI detection referenced to the number of N_2O_5 molecules taken up within a given time, usually 500 s. The corresponding twin product not directly detected by REMPI, for instance NO in the case of REMPI detection of NO_2, was evaluated as described above from the MS spectra. At low concentrations up to $[N_2O_5] = 2.0 \times 10^{12}$ molecule cm^{-3} the yields of both NO and NO_2 are identical within experimental uncertainty and equal to between 80 and 100%. Beyond this threshold value of $[N_2O_5]$ the NO_2 yield detected by REMPI and the NO yield inferred from the MS spectra seem to decrease significantly. This decrease by roughly a factor of 2 seems to depend primarily on the concentration and not on the dose of N_2O_5 taken up by soot, as revealed by a comparison between lines 3 and 4 for gray soot, and between lines 5 and 6 for black soot of Table 4. The subtle difference between the effect of concentration and dose undoubtedly points toward a complex mechanism for the heterogeneous interaction of N_2O_5 with soot. A similar situation prevails for the interaction of N_2O_5 with ice at low temperatures. We conclude that both the NO and NO_2 yields tend toward 100% for the reaction of N_2O_5 on soot under atmospheric conditions, that is, for small N_2O_5 concentrations.

In addition, neither HNO_3 nor HONO was observed in any of the uptake experiments on both gray and black soot. The absence of significant amounts of HNO_3 is somewhat of a surprise because N_2O_5 is known for its efficient hydrolysis in the presence of small amounts of adsorbed water. On Norit A, a commercial carbon black product that holds important quantities of adsorbed water, the reaction of N_2O_5 generated a large yield of HNO_3[47] that was generated through heterogeneous hydrolysis of N_2O_5 in addition to the reduction of N_2O_5 resulting in NO. The equimolar formation of NO and NO_2 in the uptake

TABLE 4: Yield of NO_2 and NO Given as Percentage with Respect to the Total Number of Molecules of N_2O_5 Taken up on Gray and Black Soot during a Reaction Time of 500 s (19.6 cm^2 Geometric Surface Area)[a]

$[N_2O_5]_0$, cm^{-3}	$N_2O_{5(lost)}$ (gray soot)	$NO_{2(g)}$ (gray soot)	% yield	$NO_{(g)}$ (gray soot)	% yield
$(1.0 \pm 0.5) \times 10^{12}$ [b]	$(6.0 \pm 1.5) \times 10^{17}$	*$(4.8 \pm 1.2) \times 10^{17}$*	*80*	$(4.3 \pm 1.3) \times 10^{17}$	72
$(1.6 \pm 0.5) \times 10^{12}$ [b]	$(8.9 \pm 1.3) \times 10^{17}$	$(7.7 \pm 1.6) \times 10^{17}$	86	*$(8.0 \pm 1.1) \times 10^{17}$*	*90*
$(2.0 \pm 0.7) \times 10^{12}$ [b]	$(9.8 \pm 1.1) \times 10^{17}$	$(9.3 \pm 1.5) \times 10^{17}$	94	*$(8.6 \pm 0.9) \times 10^{17}$*	*88*
$(2.7 \pm 1.0) \times 10^{12}$ [b]	$(1.0 \pm 0.2) \times 10^{18}$	$(4.5 \pm 0.2) \times 10^{17}$	45	*$(3.8 \pm 0.7) \times 10^{17}$*	*38*
$(8.0 \pm 1.3) \times 10^{12}$ [c]	$(2.0 \pm 0.3) \times 10^{18}$	$(7.0 \pm 1.2) \times 10^{17}$	33	*$(7.0 \pm 1.0) \times 10^{17}$*	*35*
$[N_2O_5]_0$, cm^{-3}	$N_2O_{5(lost)}$ (black soot)	$NO_{2(g)}$ (black soot)	% yield	$NO_{(g)}$ (black soot)	% yield
$(1.0 \pm 0.5) \times 10^{12}$ [b]	$(5.3 \pm 1.4) \times 10^{17}$	*$(5.2 \pm 1.3) \times 10^{17}$*	*98*	$(5.2 \pm 1.5) \times 10^{17}$	100
$(1.3 \pm 0.7) \times 10^{12}$ [b]	$(9.5 \pm 1.5) \times 10^{17}$	*$(8.2 \pm 1.3) \times 10^{17}$*	*87*	$(7.7 \pm 1.2) \times 10^{17}$	81
$(1.5 \pm 0.5) \times 10^{12}$ [b]	$(1.0 \pm 0.7) \times 10^{18}$	*$(9.5 \pm 1.9) \times 10^{17}$*	*95*	$(9.9 \pm 0.5) \times 10^{17}$	100
$(1.9 \pm 0.8) \times 10^{12}$ [b]	$(9.7 \pm 1.2) \times 10^{17}$	*$(8.7 \pm 1.0) \times 10^{17}$*	*90*	$(8.2 \pm 1.0) \times 10^{17}$	84
$(2.0 \pm 0.8) \times 10^{12}$ [b]	$(1.0 \pm 0.2) \times 10^{18}$	$(9.6 \pm 1.1) \times 10^{17}$	92	*$(8.7 \pm 1.7) \times 10^{17}$*	*87*
$(2.9 \pm 1.0) \times 10^{12}$ [b]	$(1.0 \pm 0.3) \times 10^{18}$	$(4.2 \pm 1.2) \times 10^{17}$	45	*$(5.0 \pm 1.5) \times 10^{17}$*	*50*
$(8.0 \pm 1.3) \times 10^{12}$ [c]	$(1.7 \pm 0.5) \times 10^{18}$	$(6.6 \pm 1.1) \times 10^{17}$	39	*$(7.1 \pm 2.1) \times 10^{17}$*	*42*

[a] The data for NO and NO_2 given in straight font correspond to yields obtained by REMPI detection whereas data listed in italics have been obtained using the analysis of MS signals at *m/e* 30 and 46 (see Appendix A2). [b] Orifice diameter = 8 mm. [c] Orifice diameter = 4 mm.

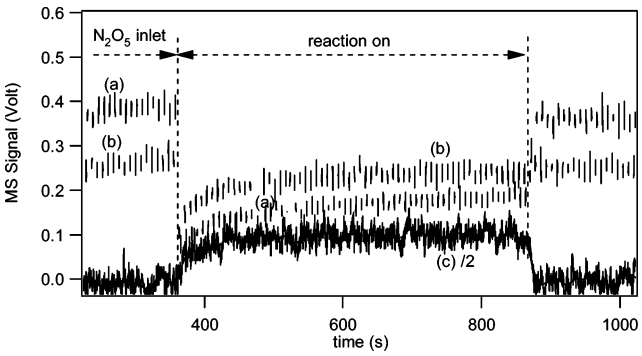

Figure 8. N_2O_5 uptake on a sample of 15 mg of black soot at $[N_2O_5] = (2.0 \pm 0.7) \times 10^{12}$ cm^{-3} and at an orifice diameter of 8 mm. Curves a and b correspond to the raw MS signals monitored at *m/e* 46 and 30, respectively. Curve c corresponds to the raw REMPI signal for NO detection at $\lambda_{NO} = 452.6$ nm (Coumarin 47, Radiant Dyes) scaled to a MS signal at *m/e* 30.

of N_2O_5 on both gray and black soot suggests the occurrence of reactions 9 and 9a.

$$N_2O_{5(ads)} + \{C\} \rightarrow N_2O_{3(ads)} + \{C \cdot O_2\} \quad (9)$$

$$N_2O_{3(ads)} \rightarrow NO + NO_2 \quad (9a)$$

This mode of decomposition is similar to NO_3 decomposition according to eq 7 in that two O atoms are transferred to the soot substrate after reaction corresponding to a reduction involving the transfer of two electrons per N atom in the case of N_2O_5. In case the reduction of N_2O_5 on soot occurs via NO_2 and subsequent secondary reduction of NO_2 to NO akin to NO_2 reduction on amorphous carbon[32] it would be highly improbable to observe equimolar amounts of NO and NO_2.

3.4. Uptake Kinetics of NO_3 on Decane Soot. The interaction of NO_3 with gray and black decane soot shows that after an initial fast uptake of NO_3 there is no saturation of the sample at steady-state conditions. Figure 9 and Table 5 display the values of γ_{ss} as a function of $[NO_3]$ for gray and black soot based on the geometric sample surface of 19.6 cm^2. The uncertainties for NO_3 uptake experiments were determined from the signal-to-noise ratio of the MS signal at *m/e* 62.

We note that for a variation of $[NO_3]$ between $(2.7 \pm 0.5) \times 10^{11}$ and $(7.0 \pm 1.0) \times 10^{11}$ cm^{-3} γ_{ss} decreases from 0.2 ± 0.03 to 0.11 ± 0.01 for both types of soot. Variations of $[NO_3]$ between $(7.0 \pm 1.0) \times 10^{11}$ cm^{-3} and $(2.3 \pm 0.5) \times 10^{12}$ cm^{-3} result in a constant value of $\gamma_{ss} = (6.5 \pm 1.5) \times 10^{-2}$, independent of $[NO_3]$. In addition, there is no significant difference in γ_{ss} between gray and black soot.

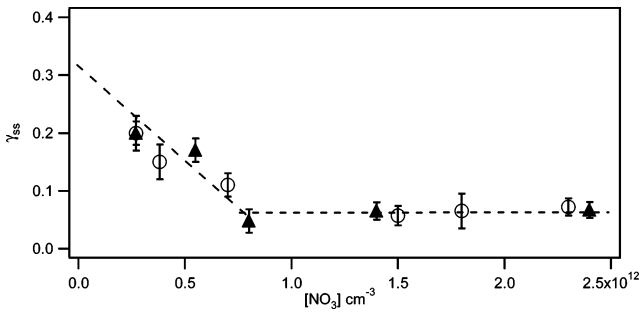

Figure 9. Uptake coefficient γ_{ss} of NO_3 based on the geometric sample surface as a function of $[NO_3]$ (orifice diameter = 8 mm): NO_3 on black (triangles) and gray soot (open circles).

TABLE 5: Summary of Uptake Experiments of NO_3 on 10 mg of Gray and Black Decane Soot[a]

$[NO_3]_0$, cm^{-3}	γ_0 (gray soot)	γ_{ss} (gray soot)
$(2.7 \pm 0.5) \times 10^{11}$	0.44 ± 0.05	0.2 ± 0.02
$(3.8 \pm 1.8) \times 10^{11}$	0.35 ± 0.06	0.15 ± 0.03
$(7.0 \pm 1.0) \times 10^{11}$	0.15 ± 0.07	0.11 ± 0.02
$(1.5 \pm 0.5) \times 10^{12}$	0.12 ± 0.05	$(5.7 \pm 1.3) \times 10^{-2}$
$(1.8 \pm 0.5) \times 10^{12}$	0.12 ± 0.05	$(6.5 \pm 1.0) \times 10^{-2}$
$(2.3 \pm 0.5) \times 10^{12}$	0.12 ± 0.04	$(7.2 \pm 1.5) \times 10^{-2}$
$[NO_3]_0$, cm^{-3}	γ_0 (black soot)	γ_{ss} (black soot)
$(2.7 \pm 0.5) \times 10^{11}$	0.5 ± 0.07	0.2 ± 0.03
$(5.5 \pm 1.0) \times 10^{11}$	0.35 ± 0.08	0.17 ± 0.02
$(8.0 \pm 0.5) \times 10^{11}$	0.3 ± 0.04	$(6.7 \pm 1.4) \times 10^{-2}$
$(1.4 \pm 0.5) \times 10^{12}$	0.2 ± 0.05	$(6.5 \pm 1.5) \times 10^{-2}$
$(2.3 \pm 0.5) \times 10^{12}$	0.18 ± 0.03	$(4.8 \pm 1.0) \times 10^{-2}$

[a] Initial (γ_0) and steady-state (γ_{ss}) uptake coefficients (orifice diameter = 8 mm, 19.6 cm^2 geometric surface area).

From this series of measurements it is evident that γ_{ss} follows a rate law pseudo first order in NO_3 for $[NO_3] > (7.0 \pm 1.0) \times 10^{11}$ cm^{-3}. Conversely, for $[NO_3] < (7.0 \pm 1.0) \times 10^{11}$ cm^{-3} the inverse dependence of γ_{ss} on $[NO_3]$ suggests that the mechanism of NO_3 uptake is complex and does not correspond to a simple first-order rate law for uptake. A similar behavior has been observed for the interaction of NO_3 with mineral dust substrates such as Kaolinite.[44] Akin to γ_{ss} , γ_0 for black and

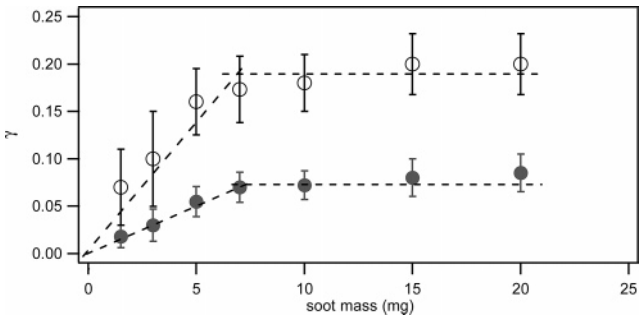

Figure 10. Uptake coefficient of NO_3 on gray soot based on the geometric sample surface: dependence of the initial (open circles) and steady-state (full circles) uptake coefficient on sample mass at $[NO_3] = (2.3 \pm 0.5) \times 10^{12}$ cm^{-3} (orifice diameter = 8 mm).

gray soot seems to follow the same trend as a function of $[NO_3]$ within experimental uncertainty.

Figure 10 displays the steady-state uptake coefficient γ_{ss} of NO_3 as a function of the mass of gray and black soot (Table 6). A linear dependence of γ_{ss} as a function of the substrate mass is clearly visible for soot masses up to 7 mg. The identical situation holds for black soot (not shown). We note that for the interaction pair NO_3−soot there is no mass dependence beyond the mass of 7 mg, which we interpret as the minimum mass required for forming a coherent monolayer of soot. The alternative interpretation of NO_3 penetrating into deeper layers of the sample is less applicable owing to the large absolute values of γ. This value of 7 mg corresponds to a soot loading of $7/19.6 = 0.37$ mg/cm^2 and is identical to that for black soot. In earlier work[21] a value for the threshold loading of 0.41 ± 0.1 mg/cm^2 has been determined. Soot is a porous material, and on the time scale of a few seconds given by the orifice diameter of the flow reactor, we do not expect NO_3 to explore the internal surface of the pores as given for instance by the BET surface area. We do not think that the surface porosity of soot plays an important role in the determination of the uptake coefficient in view of the large value of γ_{ss} of NO_3 on gray and black soot. In contrast, for the reaction of N_2O_5 on soot we may have to take into account possible diffusion of N_2O_5 into deeper sample layers due to smaller values of γ_{ss} with respect to NO_3.

We therefore take the geometric surface area for the evaluation of the gas−surface collision frequency ω under the constraint of the present experimental conditions of low gas-phase residence times for NO_3. The linear mass dependence of γ_0 and γ_{ss} observed below 7 mg for gray and black soot and displayed in Figure 10 is interpreted that no coherent layer of soot on the sample holder has been formed at those sample masses yet. Beyond 7 mg of soot the initial uptake coefficient γ_0 is very large and stays constant at approximately 0.2 such that NO_3 does not have sufficient time to explore the internal surface area of the substrate given by the BET surface. Therefore, as already discussed for N_2O_5 on mineral dust substrates, we do not think that the pore diffusion model[48] should be applied to correct γ_0 or γ_{ss}. At steady-state conditions we note that γ_{ss} follows the same trend as γ_0 as a function of mass of the soot sample. The correction to γ_{ss} afforded by the pore diffusion theory, if feasible, may serve as a lower limit for γ whereas γ_{ss} based on the geometrical surface area may be regarded as an upper limit to the true value of γ. In addition, it is noteworthy that the pore diffusion theory has never been successfully applied to soot substrates in view of their structural complexity. If we use the BET surface area to provide a lower bound for γ_{ss} of NO_3 reacting on 20 mg of soot, we obtain $\gamma_{BET} = 1.2 \times 10^{-7}$ and $\gamma_{BET} = 3.7 \times 10^{-8}$ for gray and black soot, respectively.

The amount of adsorbed NO_3 during an uptake experiment on gray and black soot turned out to be the same. At $[NO_3] = (2.3 \pm 0.5) \times 10^{12}$ cm^{-3} $(3.3 \pm 0.7) \times 10^{18}$ molecules of NO_3 were adsorbed on 10 mg of soot during a reaction time of 500 s. During this time the samples did not saturate. As discussed in recent work on the interaction of NO_3 on mineral dust,[44] NO_3 may be represented by a 4.5 Å diameter sphere with a projected surface area of 1.6×10^{-15} cm^2/molecule, which leads to a full surface coverage of 6.3×10^{14} molecules cm^{-2}. The 10 mg sample of gray soot has a total surface area of 6.9×10^3 cm^2 based on a BET surface area of 69 m^2/g (see Table 1). This leads to 1.3×10^{16} and 3.5×10^{19} NO_3 forming a monolayer on 10 mg of soot based on the geometric and BET surface area, respectively. Therefore, the total number of NO_3 taken up on the substrate during 500 s has consumed $3.3 \times 10^{18}/3.5 \times 10^{19} = 9.4\%$ of reactive sites based on the BET surface area. On the basis of this estimate, we may expect to observe increasing levels of saturation of NO_3 uptake on soot beyond 50% coverage at 2500 s of exposure at $[NO_3] = (2.3 \pm 0.5) \times 10^{12}$ cm^{-3}.

3.5. Uptake Kinetics of N_2O_5 on Decane Soot. Figure 11 and Table 7 display the kinetic results of the heterogeneous reaction of N_2O_5 on gray and black soot in terms of γ_0 and γ_{ss} based on the geometric sample surface. We note from Figure 11 that both γ_0 and γ_{ss} decrease with increasing $[N_2O_5]$ down to a constant value of 5 to 10×10^{-3} that is independent of $[N_2O_5]$ for both γ_0 and γ_{ss}. The concentration dependence of γ_0 and γ_{ss} shows the same trend as for NO_3 albeit with two differences: for one the threshold value for $[N_2O_5]$ below which the uptake coefficient increases with decreasing $[N_2O_5]$ in an inverse γ/concentration dependence is higher than for NO_3. This threshold value for black soot seems to lie around $[N_2O_5] = 3 \times 10^{12}$ molecule cm^{-3}, whereas it lies around $(7-8) \times 10^{11}$ molecule cm^{-3} for NO_3 according to Figure 9. The situation is less clear for gray soot, which seems to follow an inverse γ/concentration relationship throughout the examined concentration range where the values of γ_0 and γ_{ss} coincide at the highest examined $[N_2O_5]$ of 8×10^{12} molecule cm^{-3}. The second difference with NO_3 is the fact that the γ dependence on $[N_2O_5]$ for gray and black soot is different from that with N_2O_5 whereas it is identical for both types of soot in the case of NO_3 as displayed in Figure 9. In any case, the concentration independent γ value for N_2O_5 beyond the threshold value is a factor of 10 lower than for the corresponding γ value for NO_3. As for NO_3 we report the calculated value of γ using the BET surface area thus regarding it as a lower bound. The steady-state uptake coefficient for N_2O_5 reacting on 20 mg of soot is $\gamma_{BET} = 3.2 \times 10^{-8}$ for gray and black soot (see Table 7).

4. Conclusions and Atmospheric Significance

The reaction products resulting from the heterogeneous reaction of N_2O_5 and NO_3 with soot support the reduction of both trace gases according to reactions 9, 9a, and 7. N_2O_5 yields an equimolar amount of NO + NO_2 whereas NO_3 exclusively leads to NO independent of the type of decane soot. The nature of the reaction products reveals a heterogeneous renoxification reaction following a mechanism that effectively converts NO_y to NO_x. The science community is looking for renoxification pathways other than the photolysis of HNO_3 to adjust the $[HNO_3]/[NO_x]$ concentration ratio downward, as all models substantially overpredict HNO_3.[49] The present work does not lay any claim to the importance of these renoxification pathways but does emphasize its potential importance in certain situations.

TABLE 6: Summary of Uptake Experiments with NO_3 on Gray and Black Soot as a Function of Sample Mass ($[NO_3] = (2.3 \pm 0.5) \times 10^{12}$ cm^{-3}, Orifice Diameter = 8 mm)

mass (mg)	γ_0 (gray soot)	γ_{ss} (gray soot)	γ_0 (black soot)	γ_{ss} (black soot)
1.5	$(7.0 \pm 4.0) \times 10^{-2}$	$(1.8 \pm 1.2) \times 10^{-2}$	$(5.0 \pm 3.5) \times 10^{-2}$	$(1.5 \pm 1.3) \times 10^{-2}$
3	0.1 ± 0.05	$(3.0 \pm 1.7) \times 10^{-2}$	$(8.0 \pm 3.0) \times 10^{-2}$	$(2.5 \pm 1.3) \times 10^{-2}$
5	0.16 ± 0.035	$(5.5 \pm 1.6) \times 10^{-2}$	0.15 ± 0.035	$(5.0 \pm 1.5) \times 10^{-2}$
7	0.17 ± 0.035	$(6.5 \pm 1.6) \times 10^{-2}$		
10	0.12 ± 0.030	$(7.2 \pm 1.2) \times 10^{-2}$	0.18 ± 0.03	$(6.7 \pm 1.4) \times 10^{-2}$
15	0.2 ± 0.032	$(8.0 \pm 2.0) \times 10^{-2}$	0.2 ± 0.03	$(7.5 \pm 2.3) \times 10^{-2}$
20	0.2 ± 0.032	$(8.5 \pm 2.0) \times 10^{-2}$	0.2 ± 0.03	$(8.4 \pm 2.0) \times 10^{-2}$

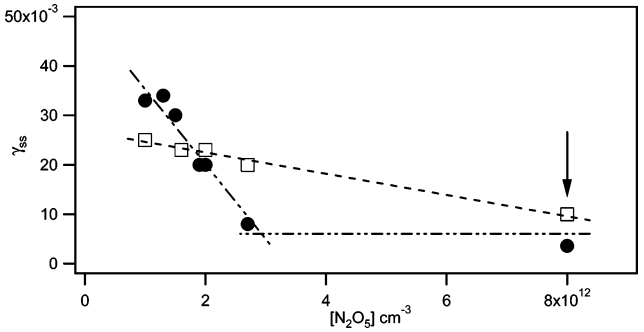

Figure 11. Uptake coefficient γ_{ss} of N_2O_5 based on the geometric sample surface as a function of $[N_2O_5]$: N_2O_5 on black (circles) and gray soot (open squares). For all measurements we used the 8 mm orifice diameter except for the point marked by the arrow where a 4 mm orifice diameter has been used.

TABLE 7: Summary of Results for Uptake Experiments of N_2O_5 on 10 mg of Gray and Black Decane Soot[a]

$[N_2O_5]_0$, cm^{-3}	γ_0 (gray soot)	γ_{ss} (gray soot)
$(1.0 \pm 0.5) \times 10^{12}$ [a]	$(8.5 \pm 0.7) \times 10^{-2}$	$(2.5 \pm 1.0) \times 10^{-2}$
$(1.6 \pm 0.5) \times 10^{12}$ [a]	$(5.4 \pm 0.3) \times 10^{-2}$	$(2.3 \pm 0.7) \times 10^{-2}$
$(2.0 \pm 0.7) \times 10^{12}$ [a]	$(5.2 \pm 0.2) \times 10^{-2}$	$(2.3 \pm 0.4) \times 10^{-2}$
$(2.7 \pm 1.0) \times 10^{12}$ [a]	$(4.6 \pm 0.5) \times 10^{-2}$	$(2.0 \pm 0.3) \times 10^{-2}$
$(8.0 \pm 1.3) \times 10^{12}$ [b]	$(4.4 \pm 0.7) \times 10^{-2}$	$(1.0 \pm 0.5) \times 10^{-2}$
$[N_2O_5]_0$ cm^{-3}	γ_0 (black soot)	γ_{ss} (black soot)
$(1.0 \pm 0.5) \times 10^{12}$ [a]	0.1 ± 0.05	$(3.3 \pm 0.8) \times 10^{-2}$
$(1.3 \pm 0.7) \times 10^{12}$ [a]	0.1 ± 0.05	$(3.4 \pm 0.5) \times 10^{-2}$
$(1.5 \pm 0.5) \times 10^{12}$ [a]	0.1 ± 0.08	$(3.0 \pm 0.6) \times 10^{-2}$
$(1.9 \pm 0.8) \times 10^{12}$ [a]	$(8.9 \pm 0.5) \times 10^{-2}$	$(2.0 \pm 0.8) \times 10^{-2}$
$(2.0 \pm 0.8) \times 10^{12}$ [a]	$(7.5 \pm 0.5) \times 10^{-2}$	$(2.0 \pm 0.5) \times 10^{-2}$
$(2.9 \pm 1.0) \times 10^{12}$ [a]	$(7.3 \pm 0.5) \times 10^{-2}$	$(8.0 \pm 1.4) \times 10^{-3}$
$(8.0 \pm 1.3) \times 10^{12}$ [b]	$(4.4 \pm 0.5) \times 10^{-2}$	$(3.6 \pm 1.0) \times 10^{-3}$

[a] Initial (γ_0) and steady-state (γ_{ss}) uptake coefficients (orifice diameter = 8 mm; orifice diameter = 4 mm).

In contrast to NO_2[21] and HNO_3[23] the mass balance for both N_2O_5 (Table 4) and NO_3 (Table 2) indicates that the yields of reaction products are independent of the type of soot, in agreement with the measured uptake coefficients that are also essentially independent of the type of soot, as displayed in Figures 9 and 11. We attribute the higher NO yield in the case of NO_3 reacting with black compared to gray decane soot to the decomposition of HONO that is formed as a consequence of the presence of NO_2 on black soot. This is an artifact of the used NO_3 source that delivers 3 times as much NO_2 compared to NO_3 and that forces us to take into account the interaction of NO_2 with soot in detail. In contrast to NO_3 and N_2O_5, the type of soot matters for the NO_2/soot interaction.[32]

The N_2O_5 yield of 23% is observed to be independent of the type of soot and is a consequence of the presence of adsorbed NO_3 reacting with excess gaseous NO_2. Adsorbed NO_2 is reacting to HONO and NO on gray and black decane soot, respectively.[22] We conclude that the extents of adsorption of NO_3 are identical on both types of soot. Somewhat surprisingly, only a very low rate of hydrolysis of N_2O_5 to HNO_3 is observed on both types of soot, which is at variance with results on N_2O_5 reacting on carbon black, Norit A, a carbonaceous material produced from pyrolysis.[47] For both trace gases significant amounts remain adsorbed on the soot substrate. Only 11 and 16% of the lost NO_3 are converted to NO on gray and black decane soot, respectively. We attribute the difference of 5% "excess" yield of NO on black vs gray soot to HONO decomposition (see above). Considering the fraction of NO_3 that goes on to yield N_2O_5 we see that approximately two-thirds of the lost NO_3 remains adsorbed on soot during uptake vs 1/3 generating gaseous N_2O_5. In contrast, we observe an essentially quantitative conversion of N_2O_5 to an equimolar mixture of NO + NO_2 for concentrations lower than 3×10^{12} molecules cm^{-3}, which means that no significant amounts of N_2O_5 remain adsorbed on both types of soot, as indicated in Table 4. At higher concentrations of N_2O_5 the rate of surface reaction according to reactions 9 and 9a obviously slows down compared to N_2O_5 adsorption which leads to a significant reduction of the product yield.

In contrast to the interaction of NO_2 and HNO_3 with gray and black hexane and decane soot[21,23] whose product branching ratio strongly depended on the type of soot, we see the opposite behavior, namely a lack of dependence on the type of soot in the case of NO_3 and N_2O_5. This finding is somewhat unexpected compared to both the behavior of NO_2 and HNO_3 and is in disagreement with the results of Smith and co-workers[24] who have observed a strong correlation of the reactivity of O_3 and of the interaction of H_2O vapor with several types of combustion soot as a function of the air/fuel ratio that is comparable to the fuel/oxygen ratio used in the present work. In general agreement with the present results Longfellow et al.[50−52] find a yield of NO_2 of 104 ± 10% and a small HONO yield on the order of 1% for the interaction of N_2O_5 on propane soot whose fuel to oxygen ratio was not controlled. The small HONO yield was believed to originate from the secondary reaction of NO_2 on propane soot. On the side, the present work yields additional confirmation of HONO formation of NO_2 on decane soot compared to previous results obtained on hexane soot[21] and lends support to the importance of the fuel to oxygen ratio λ in determining the reactivity of soot toward NO_2.[21−24]

Finally, we would like to point out that the heterogeneous reduction reaction of both NO_3 and N_2O_5 on both types of soot formally corresponds to a 4 electron transfer in regard to NO formation from NO_3 and NO + NO_2 formation from N_2O_5. This is accompanied with the formal transfer of two O atoms from the reacting trace gas to the reducing soot substrate. In contrast, HONO formation from NO_2 implies a formal transfer of one electron,[21,22,40,41] whereas HONO formation from HNO_3/soot interaction[21] requires the transfer of two electrons. In this analysis we regard the NO formation from the NO_2/black decane soot interaction as a secondary product of HONO decomposition on soot,[22] i.e., a one-electron reduction.

From the present kinetic uptake experiments performed on gray and black decane soot, we may extrapolate γ to vanishing NO_3 concentration as displayed in Figure 9 and obtain an estimate of γ_{ss} for $[NO_3] < 7.0 \times 10^{11}$ molecule cm^{-3} independent of the type of soot. With tropospheric $[NO_3]$ at a typical value of 2.0×10^9 molecule cm^{-3},[30] γ_{ss} tends toward values larger than 0.3 according to the results displayed in Figure 9. The NO_3 loss rate constant (k_{het}) due to heterogeneous uptake onto aerosols is given by $k_{het} = \tau^{-1}(NO_3) = \gamma A\bar{c}/4V$ as far as the surface resistance is concerned without consideration of mass transfer, where γ is the uptake coefficient of NO_3, A/V is the surface-to-volume ratio of the aerosol, and $\bar{c}$ is the mean molecular speed of NO_3.

The uptake of NO_3 on soot was studied in a large aerosol chamber and yielded an upper limit of $\gamma \leq 3.0 \times 10^{-4}$ at very low relative humidity (rh) ($H_2O < 10$ ppm), whereas at 50% rh an upper limit of $\gamma \leq 1.0 \times 10^{-3}$ was obtained. These values are 2 (50% rh) and 3 orders of magnitude lower than the γ value of 0.3 for $[NO_3] < 7.0 \times 10^{11}$ molecule cm^{-3}. The impact of soot aerosol surface reactions on the rate of formation of photochemical ozone was also investigated using a box model.[11] The results showed that soot has a minor impact on ozone formation at low $[NO_y]$. In contrast, soot may cause an ozone reduction of up to 10% at high $[NO_y]$. However, we must point out that the nature of the carbonaceous aerosol from a spark ignition generator[11] is significantly different from flame soot used in the present study. At variance, the work of Saathoff et al.[11] shows that the uptake of NO_3 on soot seems to saturate and tend to a small γ_{ss} value at steady state. This may perhaps be due to the graphitic core of the used soot that proves to be unreactive toward NO_3 free radical attack once the reactive "soot" surface functionalities are consumed and the "bare" graphitic core is exposed. On the other hand, the present experiments are not sensitive to saturation phenomena owing to the shorter time scale used such that critical comparison of results has to await further experiments.

Acknowledgment. We gratefully acknowledge the Fonds National Suisse de la Recherche Scientifique (FNS) for generous support of this research under project no. 200020-105471/1 as well as OFES, now SER (Secrétariat de l'enseignement et de la recherche), for financing the Swiss participation of the MINATROC project within the fifth framework program of the European Union (EU).

Appendix A: Data Analysis for the Detection of Reaction Products

A1. NO_3 Reaction and Detection. The absolute NO_2 concentration $[NO_2]_{0(REMPI)}$ originating from the NO_3 source has been determined by means of in situ REMPI detection akin to the method outlined in ref 44. Subsequently, the corresponding MS signal of NO_2 at *m*/*e* 46, $I_{0(REMPI)}^{46(NO_2)}$, was calculated according to eq A3 (see below). We point out that in contrast to MS signals that are proportional to an ion current, and thus to flux, the REMPI signals scale with the concentration of the detected trace gas as explained in detail in ref 44.

Through a calibrated mass spectrum of pure HNO_3 we have accurately determined the contribution of the HNO_3 impurity at *m*/*e* 46 and 30 by using the fragmentation pattern expressed as the ratios

$$f_{46} = \frac{I_0^{46(HNO_3)}}{I_o^{63(HNO_3)}} = 52 \pm 8 \qquad f_{30} = \frac{I_0^{30(HNO_3)}}{I_o^{63(HNO_3)}} = 33 \pm 4$$

In the absence of a substrate, $f_{46}I_0^{63(HNO_3)}$ and $f_{30}I_0^{63(HNO_3)}$ have been subtracted from the total MS signals I_0^{46} and I_0^{30} at *m*/*e* 46 and 30, respectively, to assign the remaining MS amplitude to the NO_2^+ and NO^+ fragments of N_2O_5: $I_0^{46(N_2O_5)} = I_0^{46} - f_{46}I_0^{63(HNO_3)}$ and $I_0^{30(N_2O_5)} = I_0^{30} - f_{30}I_0^{63(HNO_3)}$. The same type of procedure has been used for experiments in the presence of a sample once all the reaction products were known, starting at the high mass end (HNO_3, NO_3, HONO, N_2O_5, NO_2, and NO).

In the absence of the soot substrate, $I_{0(REMPI)}^{46(NO_2)}$ and $f_{46}I_0^{63(HNO_3)}$ have been subtracted from the total MS signal I_0^{46} at *m*/*e* 46 to attribute the remaining signal to the NO_2^+ fragment of the electron-impact ionization of NO_3 once the absence of nondissociated N_2O_5 from the NO_3 source was established. The temperature of the NO_3 source was increased to the point where all non dissociated N_2O_5 fell below the detection limit. The resulting MS signal at *m*/*e* 46 pertaining to NO_3 is $I_0^{46(NO_3)} = I_0^{46} - I_{0(REMPI)}^{46(NO_2)} - f_{46}I_0^{63(HNO_3)}$.

When soot is exposed to the effluents of the NO_3 source, NO_3 is taken up and reacts on soot, resulting in a decrease of $[NO_3]$ that leads to a concomitant decrease of the MS signal I_r^{46} at *m*/*e* 46. To correct for the contribution of NO_3 at *m*/*e* 46 for the following series of uptake experiments, we have determined $r_{46} = I_0^{46(NO_3)}/I_0^{62(NO_3)} = 8.5 \pm 1.5$ as the ratio of the MS signal $I_0^{46(NO_3)}$ at *m*/*e* 46 (NO_2^+) and $I_0^{62(NO_3)}$, the molecular ion peak at *m*/*e* 62 (NO_3^+), both for NO_3 free radical in the absence of the soot sample.

As a result of the exposure of the sample to NO_3 in the presence of NO_2, we expect four possible reaction products besides changes of NO_2: HNO_3, N_2O_5, HONO, and NO. Under our experimental conditions HNO_3 may possibly be formed at high densities by heterogeneous recombination of NO_2 and NO_3 to N_2O_5 and subsequent heterogeneous hydrolysis. To find other possible reaction products contributing to the I_{exc}^{46} MS signal intensity at *m*/*e* 46 not due to HNO_3, we have subtracted the following known contributions from the total MS signal I_r^{46}: (a) $I_{r(REMPI)}^{46(NO_2)}$ for NO_2, (b) $r_{46}I_r^{62(NO_3)}$ for NO_3, and (c) $f_{46}I_r^{63(HNO_3)}$ for the possible HNO_3 formation during the reaction which result in the following remaining MS signal called excess MS intensity at *m*/*e* 46:

$$I_{exc}^{46} = I_r^{46} - I_{r(REMPI)}^{46(NO_2)} - r_{46}I_r^{62(NO_3)} - f_{46}I_r^{63(HNO_3)} \quad \text{(A1)}$$

It is reasonable to expect that N_2O_5 may be the only reaction product contributing to an excess at *m*/*e* 46, as will be discussed below. Therefore, in the following I_{exc}^{46} will be named $I_{exc}^{46(N_2O_5)}$.

Using REMPI detection at $\lambda_{NO} = 452.6$ nm, we could not detect any NO product formation because its concentration dropped below the detection limit given by the chosen experimental conditions. Therefore, to establish the amount of NO from the excess MS signal intensity at *m*/*e* 30, I_{exc}^{30}, during the exposure of soot to NO_3, we have accurately determined all the possible contributions to the total MS signal I_r^{30} at *m*/*e* 30. The major contribution to I_r^{30} comes from the mixture of NO_2 and NO_3 originating from the hot NO_3 source given that the amount of HNO_3 and N_2O_5 in the presence of the sample is small. Using a reference mass spectrum of pure NO_2, we have calculated the effective contribution of NO_2 at *m*/*e* 30 by using the fragmentation pattern expressed as the ratio

$$z_1 = \frac{I_0^{30(NO_2)}}{I_0^{46(NO_2)}} = 2.0 \pm 0.2$$

The ratio of the MS signal $I_0^{30(NO_3)}$ at *m*/*e* 30 (NO^+) and $I_0^{62(NO_3)}$ at *m*/*e* 62 (NO_3^+) for NO_3 radical has been defined as follows:

$$r_{30} = \frac{I_0^{30(NO_3)}}{I_0^{62(NO_3)}} = \frac{I_0^{30} - z_1 I_0^{46(NO_2)} - f_{30} I_0^{63(HNO_3)}}{I_0^{62(NO_3)}} = 6.3 \pm 0.8$$

where I_0^{30} is the total MS signal at *m*/*e* 30 and $z_1 I_0^{46(NO_2)}$ and f_{30} $I_0^{63(HNO_3)}$ are the contributions of NO_2 and HNO_3, both at *m*/*e* 30, respectively.

As explained above, it is reasonable to expect that N_2O_5 will be a reaction product of the reaction of NO_3 on soot. However, we have to consider that pure N_2O_5 has fragment peaks at *m*/*e* 46 and 30 that are correlated by the fragmentation pattern expressed as the ratio $r_{N_2O_5} = I_0^{46(N_2O_5)}/I_0^{30(N_2O_5)} = 1.36 \pm 0.3$.

This ratio was established after extensive passivation of the inlet system and running the NO_3 source at ambient temperature to afford a stabilized flow of N_2O_5. As shown in previous studies on soot,[23] HNO_3 reacts on the soot surface resulting in the formation of volatile products such as HONO and NO that contribute to the total MS signal I_r^{30} at *m*/*e* 30. At the present experimental conditions HONO has a measurable, albeit low intensity, parent peak at *m*/*e* 47 ($HONO^+$). Therefore, the effective contribution of HONO at *m*/*e* 30 has been determined by using its fragmentation pattern expressed as the ratio $h = I_0^{30(HONO)}/I_0^{47(HONO)} = 22 \pm 0.5$. As already explained above, HNO_3 present in the hot NO_3 source also provides a contribution to the MS amplitude at *m*/*e* 30 as expressed by f_{30}.

Finally, during the exposure of soot to NO_3 we have subtracted the following known contributions from the total MS signal I_r^{30} at *m*/*e* 30: (a) $I_{exc}^{46}/r_{N_2O_5}$ for the contribution owing to the presence of N_2O_5, (b) $z_1 I_{r(REMPI)}^{46(NO_2)}$ for the contribution of NO_2 (see eq A3, next paragraph), (c) $r_{30} I_r^{62(NO_3)}$ for the contribution of NO_3, (d) $h I_r^{47(HONO)}$ for HONO, (e) $f_{30} I_r^{63(HNO_3)}$ for HNO_3. The final expression for the residual (=excess) MS signal amplitude I_{exc}^{30} attributed to the presence of NO resulted from the following equation:

$$I_{exc}^{30} = I_r^{30} - \frac{I_{exc}^{46(N_2O_5)}}{r_{N_2O_5}} - z_1 I_{r(REMPI)}^{(46)NO_2} - r_{30} I_r^{62(NO_3)} - h I_r^{47(HONO)} - f_{30} I_r^{63(HNO_3)} \quad \text{(A2)}$$

It is reasonable to expect that N_2O_5 and NO may be the only reaction products contributing to *m*/*e* 46 and 30, respectively, after subtraction of all known contributions to these masses displayed in eqs A1 and A2.

A2. N_2O_5 Reaction and Detection. For N_2O_5 uptake experiments performed on gray and black soot, both NO_2 and NO could be observed in the gas phase. The NO REMPI detection sensitivity was increased in the N_2O_5 uptake experiments such that both products could be detected in situ in back-to-back experiments, albeit not concurrently. The reaction product not determined using REMPI was quantified using MS signal analysis of amplitudes at *m*/*e* 30 and 46. The absolute NO and NO_2 concentrations obtained using REMPI detection were then scaled to the corresponding flow rates using eq A3 for NO_2 and the analogous expression for NO. The relevant MS calibration factors were previously established in ancillary experiments (see above).

The corresponding MS signal contribution $I_{0,r(REMPI)}^{46(NO_2)}$ at *m*/*e* 46 in the absence (subscript "0") and presence (subscript "r") of the soot sample, the NO_2 REMPI signal was scaled to a MS signal using the following equation:

$$I_{0,r(REMPI)}^{46(NO_2)} = \frac{F_{0,r}^{NO_2}}{C_{cal(NO_2)}} = \frac{[NO_2]_{0,r(REMPI)} k_{esc(NO_2)} V_{cell}}{C_{cal(NO_2)}} \quad \text{(A3)}$$

where $C_{cal(NO_2)}$ is the NO_2 calibration factor that was directly determined from an absolute measurement of $[NO_2]$ in an ancillary experiment using a suitably calibrated MS signal for pure NO_2. $k_{esc(NO_2)}$ is the NO_2 effusive loss rate constant. One should be reminded that the conversion following eq A3 is necessary because the REMPI signal scales with the concentration whereas the MS signal corresponds to a flux (see above).

Equation A3 allows one to calculate the fraction of the MS signal at *m*/*e* 46 owing to the presence of NO_2 using the measured REMPI signal for NO_2 to establish its absolute concentration. Therefore, we have corrected the MS signal at *m*/*e* 46 for the presence of NO_2 according to eq A4 when the sample is exposed to N_2O_5 and obtained the MS signal at *m*/*e* 46 for pure N_2O_5 under the assumption that there are no additional contributions to I_r^{46}.

$$I_r^{46(N_2O_5)} = I_0^{46} - I_{r(REMPI)}^{46(NO_2)} \quad \text{(A4)}$$

which thus exclusively corresponds to N_2O_5 for this experiment after correction of the MS signal I_r^{46} at *m*/*e* 46 for the contribution of NO_2 produced during uptake of N_2O_5 on the soot substrate. Specifically, significant amounts of HNO_3 were not detected in the present experiments.

To calculate the amount of NO_2 formed during the reaction of N_2O_5 on gray and black soot, we have subtracted the contribution of N_2O_5 from the total MS signal at *m*/*e* 46. The MS signal at *m*/*e* 30 was corrected for its NO contribution when NO was detected by REMPI, namely, $I_{r(REMPI)}^{30(NO)}$, after scaling to a flow rate or MS signal. Therefore, the total contribution of N_2O_5 to the MS signal at *m*/*e* 46 was $r_{N_2O_5}(I_r^{30} - I_{r(REMPI)}^{30(NO)})$. The final expression for I_{exc}^{46} attributed to the presence of NO_2 is given by eq A5.

$$I_{exc}^{46} = I_r^{46} - r_{N_2O_5}(I_r^{30} - I_{r(REMPI)}^{30(NO)}) \quad \text{(A5)}$$

Conversely, to calculate the amount of NO formed during the reaction of N_2O_5 on gray and black soot, we have subtracted the contribution of N_2O_5 from the total MS signal at *m*/*e* 30. The MS signal at *m*/*e* 46 was corrected for its NO_2 contribution when NO_2 was detected by REMPI, namely, $I_{r(REMPI)}^{(NO_2)46}$ after scaling to a flow rate or MS signal. Therefore, the total contribution of N_2O_5 to the MS signal at *m*/*e* 30 was $(I_r^{46} - I_{r(REMPI)}^{46(NO_2)})/r_{N_2O_5}$. The final expression for I_{exc}^{30} attributed to the presence of NO is given by eq A6.

$$I_{exc}^{30} = I_r^{30} - \frac{(I_r^{46} - I_{r(REMPI)}^{46(NO_2)})}{r_{N_2O_5}} \quad \text{(A6)}$$

This analysis makes use of the observation that both HNO_3 and HONO were undetectable during uptake of N_2O_5 on gray and black soot.

References and Notes

(1) Houghton, J., et al., Eds. *Climate Change 2001, The Scientific Basis*; Cambridge University Press: Cambridge, U.K., 2001.

(2) Goldberg, E. D. *Black Carbon in the Environment* John Wiley and Sons: New York, 1985.

(3) Buseck, P. R.; Posfai, M. *Proc. Natl. Acad. Sci. U.S.A.* **1999**, *96*, 3372.
(4) Posfai, M.; Simonics, R.; Li, J.; Hobbs, P. V.; Buseck, P. R. *J. Geophys. Res.—Atmos.* **2003**, *108*.
(5) Hallett, J.; Hudson, J. G.; Rogers, C. F. *Aerosol Sci. Technol.* **1989**, *10*, 70.
(6) Jensen, E. J.; Toon, O. B. *Geophys. Res. Lett.* **1997**, *24*, 249.
(7) Horvath, H. *Atmos. Environ. Pt. A—Gen. Top.* **1993**, *27*, 293.
(8) Haywood, J. M.; Ramaswamy, V. *J. Geophys. Res.—Atmos.* **1998**, *103*, 6043.
(9) Schurath, U.; Naumann, K. H. *Pure Appl. Chem.* **1998**, *70*, 1353.
(10) Kamm, S.; Möhler, O.; Naumann, K. H.; Saathoff, H.; Schurath, U. *Atmos. Environ.* **1999**, *33*, 4651.
(11) Saathoff, H.; Naumann, K. H.; Riemer, N.; Kamm, S.; Möhler, O.; Schurath, U.; Vogel, H.; Vogel, B. *Geophys. Res. Lett.* **2001**, *28*, 1957.
(12) Kirchner, U.; Scheer, V.; Vogt, R. *J. Phys. Chem. A* **2000**, *104*, 8908.
(13) IUPAC. http://www.iupac-kinetic.ch.cam.ac.uk/.
(14) Pope, C. A.; Thun, M. J.; Namboodiri, M. M.; Dockery, D. W.; Evans, J. S.; Speizer, F. E.; Heath, C. W. *Am. J. Respir. Crit. Care Med.* **1995**, *151*, 669.
(15) Pope, C. A.; Burnett, R. T.; Thurston, G. D.; Thun, M. J.; Calle, E. E.; Krewski, D.; Godleski, J. J. *Circulation* **2004**, *109*, 71.
(16) Akhter, M. S.; Chughtai, A. R.; Smith, D. M. *Appl. Spectrosc.* **1985**, *39*, 143.
(17) Bockhorn, H. In *Soot Formation in Combustion: Mechanisms and Models*; Bockhorn, H. Ed.; Springer-Verlag: Berlin, Heidelberg, 1994.
(18) Sergides, C. A.; Jassim, J. A.; Chughtai, A. R.; Smith, D. M. *Appl. Spectrosc.* **1987**, *41*, 482.
(19) Pöschl, U.; Letzel, T.; Schauer, C.; Niessner, R. *J. Phys. Chem. A* **2001**, *105*, 4029.
(20) Esteve, W.; Budzinski, H.; Villenave, E. *Atmos. Environ.* **2006**, *40*, 201.
(21) Salgado, M. S.; Rossi, M. J. *Int. J. Chem. Kinet.* **2002**, *34*, 620.
(22) Stadler, D.; Rossi, M. J. *Phys. Chem. Chem. Phys.* **2000**, *2*, 5420.
(23) Munoz, M. S. S.; Rossi, M. J. *Phys. Chem. Chem. Phys.* **2002**, *4*, 5110.
(24) Chughtai, A. R.; Kim, J. M.; Smith, D. M. *J. Atmos. Chem.* **2002**, *43*, 21.
(25) Novakov, T.; Ramanathan, V.; Hansen, J. E.; Kirchstetter, T. W.; Sato, M.; Sinton, J. E.; Sathaye, J. A. *Geophys. Res. Lett.* **2003**, *30*.
(26) Penner, J. E.; Eddleman, H.; Novakov, T. *Atmos. Environ. Pt. A—Gen. Top.* **1993**, *27*, 1277.
(27) Bodhaine, B. A. *J. Geophys. Res.—Atmos.* **1995**, *100*, 8967.
(28) Clarke, A. D. *Aerosol Sci. Technol.* **1989**, *10*, 161.
(29) Rau, J. A.; Khalil, M. A. K. *Atmos. Environ. Pt. A—Gen. Top.* **1993**, *27*, 1297.
(30) Brown, S. S.; Dube, W. P.; Osthoff, H. D.; Wolfe, D. E.; Angevine, W. M.; Ravishankara, A. R. *Atmos. Chem. Phys. Discuss.* **2006**, *6*, 9431.
(31) Kleffmann, J.; Becker, K. H.; Lackhoff, M.; Wiesen, P. *Phys. Chem. Chem. Phys.* **1999**, *1*, 5443.
(32) Tabor, K.; Gutzwiller, L.; Rossi, M. J. *J. Phys. Chem.* **1994**, *98*, 6172.
(33) Rogaski, C. A.; Golden, D. M.; Williams, L. R. *Geophys. Res. Lett.* **1997**, *24*, 381.
(34) Gerecke, A.; Thielmann, A.; Gutzwiller, L.; Rossi, M. J. *Geophys. Res. Lett.* **1998**, *25*, 2453.
(35) Kalberer, M.; Ammann, M.; Arens, F.; Gäggeler, H. W.; Baltensperger, U. *J. Geophys. Res.—Atmos.* **1999**, *104*, 13825.
(36) Kirchstetter, T. W.; Harley, R. A.; Littlejohn, D. *Environ. Sci. Technol.* **1996**, *30*, 2843.
(37) Finlayson-Pitts, B. J.; Pitts, J. N. *Science* **1997**, *276*, 1045.
(38) Staffelbach, T.; Neftel, A.; Blatter, A.; Gut, A.; Fahrni, M.; Stähelin, J.; Prevôt, A.; Hering, A.; Lehning, M.; Neininger, B.; Bäumle, M.; Kok, G. L.; Dommen, J.; Hutterli, M.; Anklin, M. *J. Geophys. Res.—Atmos.* **1997**, *102*, 23345.
(39) Sakamaki, F.; Hatakeyama, S.; Akimoto, H. *Int. J. Chem. Kinet.* **1983**, *15*, 1013.
(40) Stemmler, K.; Ammann, M.; Donders, C.; Kleffmann, J.; George, C. *Nature* **2006**, *440*, 195.
(41) Bartels-Rausch, T.; Donaldson, D. J. *Atmos. Chem. Phys. Discuss* **2006**, *6*, 10713.
(42) Takenaka, N.; Rossi, M. J. *J. Atmos. Chem.* **2005**, *50*, 171.
(43) Caloz, F.; Fenter, F. F.; Tabor, K. D.; Rossi, M. J. *Rev. Sci. Instrum.* **1997**, *68*, 3172.
(44) Karagulian, F.; Rossi, M. J. *Phys. Chem. Chem. Phys.* **2005**, *7*, 3150.
(45) Hanisch, F.; Crowley, J. N. *Phys. Chem. Chem. Phys.* **2001 b**, *3*, 2474.
(46) Ammann, M.; Kalberer, M.; Jost, D. T.; Tobler, L.; Rössler, E.; Piguet, D.; Gäggeler, H. W.; Baltensperger, U. *Nature* **1998**, *395*, 157.
(47) Brouwer, L.; Rossi, M. J.; Golden, D. M. *J. Phys. Chem.* **1986**, *90*, 4599.
(48) Keyser, L. F.; Moore, S. B.; Leu, M. T. *J. Phys. Chem.* **1991**, *95*, 5496.
(49) Rivera-Figueroa, A. M.; Sumner, A. L.; Finlayson-Pitts, B. J. *Environ. Sci. Technol.* **2003**, *37*, 548.
(50) Longfellow, C. A.; Ravishankara, A. R.; Hanson, D. R. *J. Geophys. Res.—Atmos.* **2000**, *105*, 24345.
(51) Berner, A.; Sidla, S.; Galambos, Z.; Kruisz, C.; Hitzenberger, R.; tenBrink, H. M.; Kos, G. P. A. *J. Geophys. Res.—Atmos.* **1996**, *101*, 19559.
(52) Martinez, M.; Perner, D.; Hackenthal, E. M.; Kulzer, S.; Schütz, L. *J. Geophys. Res.—Atmos.* **2000**, *105*, 22685.